[redacted]

Category: HEALTH AND SAFETY

n/a

CEX-62.81 (Final)

CIVIL EFFECTS EXERCISE

GROUND ROUGHNESS EFFECTS ON THE ENERGY AND ANGULAR DISTRIBUTION OF GAMMA RADIATION FROM FALLOUT

C. M. Huddleston, Z. G. Burson, R. M. Kinkaid, and Q. G. Klingler

Issuance Date: July 1964

CIVIL EFFECTS TEST OPERATIONS
U.S. ATOMIC ENERGY COMMISSION

NOTICE

This report is published in the interest of providing information which may prove of value to the reader in his study of effects data derived principally from nuclear weapons tests and from experiments designed to duplicate various characteristics of nuclear weapons.

This document is based on information available at the time of preparation which may have subsequently been expanded and re-evaluated. Also, in preparing this report for publication, some classified material may have been removed. Users are cautioned to avoid interpretations and conclusions based on unknown or incomplete data.

LEGAL NOTICE

PRINTED IN USA
Price $1.75. Available from the Office of
Technical Services, Department of Commerce,
Washington 25, D. C.

REYNOLDS ELECTRICAL & ENGINEERING CO., INC.
AEC CONTRACT AT(29-2)-162
MERCURY, NEVADA

CEX–62.81
CIVIL EFFECTS STUDY

GROUND ROUGHNESS EFFECTS ON THE ENERGY AND ANGULAR DISTRIBUTION OF GAMMA RADIATION FROM FALLOUT

by
C. M. Huddleston
(U. S. Naval Civil Engineering
Laboratory, Port Hueneme, California)
Z. G. Burson
R. M. Kinkaid
Q. G. Klingler

Approved by: L. J. Deal
Chief, Civil Effects Branch

Edgerton, Germeshausen & Grier, Inc.
Las Vegas, Nevada
December 1963

CONTENTS

ILLUSTRATIONS

ILLUSTRATIONS (Continued)

TABLES

ABSTRACT

The effect of ground roughness, or surface irregularities, on the radiation field above ground which had been contaminated with fallout from the explosion in the atmosphere of a nuclear device (Smallboy Event) was investigated for three types of Nevada terrain: (1) a flat dry-lake bed, (2) a plowed field with a known and uniform degree of roughness, and (3) typical wild desert. A modified 5-ton Navy 6x6 truck was used as a mobile laboratory. A collimator and a scintillation crystal with a 512-channel analyzer were used to measure gamma-ray spectra at various polar angles. Dose-vs-height measurements were also made up to a height of 40 ft.

The gamma-ray pulse-height distributions were unfolded to give energy spectra from which the angular distribution of radiation dose was calculated. Comparisons were made between theoretical predictions and these experimental determinations of directional dose.

The project was undertaken to determine the importance of ground roughness as a factor in shielding against fallout radiation.

ACKNOWLEDGEMENTS

The authors wish to express their appreciation to the following persons who contributed to the execution of the project:

L. J. Deal, Chief Civil Effects Branch, Division of Biology and Medicine, U. S. Atomic Energy Commission, for his personal initiative and continued interest which made this work possible.

John Auxier, Oak Ridge National Laboratory, for his suggestion of the project and the many useful ideas he contributed to the planning of the experiment.

The U. S. Naval Civil Engineering Laboratory, for lending the truck used in field operations.

W. G. Markland and P. C. Murphy, Edgerton, Germeshausen & Grier, Inc. (EG&G) for valuable assistance in the operational phases of the experiment.

W. E. Page, EG&G, for important contributions to the reduction of data.

Harry R. Littrell and David L. Barnhill, Analysis Group, EG&G, for their valuable contributions in preparation of computer programs for calculations of energy spectra.

Personnel of EG&G, Santa Barbara, for the design and construction of the collimator used for field measurements.

Dr. L. V. Spencer, Ottawa University, for his theoretical calculations of the angular distributions of fallout radiation at various times after weapon detonation.

Chapter 1

INTRODUCTION

The importance of ground roughness as a mechanism for natural shielding from fallout radiation has long been recognized[1]; i.e., the intensity and the energy and angular distributions of fallout radiation would be expected to depend on irregularities of the contaminated terrain. Calculations based on the uniform distribution of fallout on the surface of a smooth infinite plane cannot be expected to yield accurate predictions regarding the radiation field above the surface of a typical natural, or built-up area that contains such irregularities as gravel, foliage, ditches, hills, fences, and curbs. In the theoretical treatment of ground-roughness shielding, it has been generally supposed that radioactivity can be considered as being mixed uniformly with soil throughout a surface layer of a smooth plane; the depth of the surface layer depends on the degree of ground roughness.

Alternatively, when fallout is treated as though it were buried beneath the surface of a smooth infinite plane[1-3], the fallout is considered to be uniformly distributed in an underground hypothetical layer of infinitesimal thickness, extending infinitely in all lateral directions. The depth of the fictitious layer is called τ and is measured in mean free paths of fallout radiation in air. The depth, τ, depends on the roughness of the ground. This simpler model is clearly preferred if it gives satisfactory agreement with experiment because the calculations involved are easier.

An earlier investigation[3] was concerned with the measurement of the angular distribution and energy distribution of fallout radiation above a nearly level desert terrain of course gravel relatively free of sage-brush. Dose-versus-height measurements were not made as a part of that investigation.

In another experiment[4], the angular distribution of dose was determined 1 m above ground that had been contaminated with Cs^{137}. In both experimental determinations of the angular distribution of dose, the dose was maximum in a direction almost parallel to the surface of the contaminated ground.

A survey of ground-roughness experiments and calculations is given by Ferguson.[5]

To determine the importance ofground roughness as a natural shielding factor, it is important to know the angular distribution of dose and the variation of dose with height above types of terrain with varying degrees of roughness. Such measurements can then be compared with theoretical predictions. Also, it is valuable in shielding calculations to know the energy spectrum of the gamma radiation. The investigation reported here was directed toward a better understanding of the ground-roughness problem, particularly the importance of ground-roughness effects on fallout-radiation fields above various types of terrain.

REFERENCES

1. C. F. Ksanda, A. Moskin, and A. E. Shapiro, *Gamma Radiations from a Rough Infinite Plane*, USNRDL-TR-108, U. S. Naval Radiological Defense Laboratory, January 1956.

2. L. V. Spencer, *Structure Shielding against Fallout Radiation from Nuclear Weapons*, NBS Monograph 42, 1962.

3. R. L. Mather, R. F. Johnson, F. M. Tomnovec, and C. S. Cook, *Gamma Radiation Field above Fallout Contaminated Ground*, Operation Teapot Report, WT-1225, May 1955.

4. C. E. Clifford, *Effects of Ground Roughness on Gamma Dose from* Cs^{137} *Contamination*, Defense Research Chemical Laboratories, Report No. 401, Ottawa, March 1963.

5. J. M. Ferguson, *Ground-Roughness Effects for Fallout-Contaminated Terrain: Comparison of Measurements and Calculations*, USNRDL-TR-645, 7 May 1963.

Chapter 2

THEORY OF THE EXPERIMENT

2.1 A DESCRIPTION OF THE ACTUAL PROBLEM

In the case where actual fallout is nonuniformly distributed over irregular terrain, an exact calculation of the energy and angular distributions of radiation incident at some point above the ground would be exceedingly complicated. Factors entering into the calculations would include: (1) the shape of the ground surface within several mean free paths of the detector, (2) the surface distribution of fallout, and (3) the energy distribution of gamma radiation emitted by fallout.

Even if it were possible to perform a detailed calculation involving microscopic surface features and allowing for the possibility that the fallout may be nonuniformly mixed with varying amounts of topsoil, for variation in the gamma-ray spectrum of fallout radiation with time, and for the fact that not all fallout particles have the same gamma-ray emission spectrum, it is highly doubtful that such a calculation would be worthwhile. A detailed calculation of this type would probably be prohibitively difficult, and results obtained would apply only for the specific cases treated.

On the other hand, it is possible to make some simplifying assumptions and approximations so that the problem can be handled with relative ease and, at the same time, theoretical results may be obtained which bear enough resemblance to reality to be useful.

2.2 INFINITE-PLANE SOURCE

Begin with a treatment of an infinite-plane isotropic source of monochromatic radiation in air and compute the directly incident radiation.

The quantities r, h, and θ are as shown in the adjacent figure. It is seen that

$$di = \frac{2\pi S e^{-\tau/\cos\theta}}{4\pi(h/\cos\theta)^2} dr$$

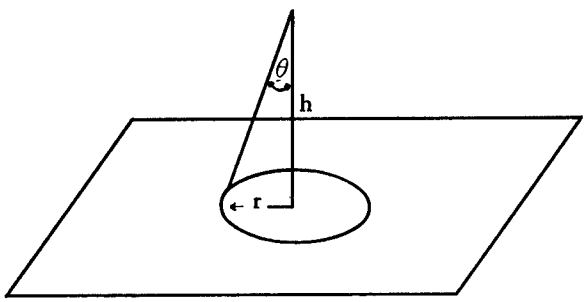

Where I = unscattered radiation intensity at the detector in photons per second per steradian

S = source strength in photons per square centimeter per second

τ = number of mean free paths of air between the source and the detector

If Ω = solid angle,

$d\Omega = 2\pi \sin\theta \, d\theta$

Noting that $r = h \tan\theta$

and $dr = h \sec^2\theta \, d\theta$

thus,
$$\frac{dI}{d\Omega} = \frac{Se^{-\tau/\cos\theta}}{4\pi\cos\theta} \qquad (2.1)$$

It should be evident that Eq. 2.1 is valid if the source is deposited in an infinite plane below a smooth infinite surface of earth, providing we understand that τ refers to the number of mean free paths of matter between the source and the detector.

2.3 APPROXIMATE TREATMENT OF GROUND ROUGHNESS EFFECTS

The case where the terrain is irregular can be treated by the approximation that the actual case is represented by an infinite-plane source buried some distance below a smooth infinite surface of earth [1]. In Fig. 2.1 are plotted a family of curves showing the relationship between $I(\theta)$ and $\cos\theta$ for various values of d, the distance in air above a smooth, infinite, fallout-contaminated plane.

Inspection of Fig. 2.1 shows that there is a value θ_{max} at which the dose is a maximum, and that θ_{max} depends upon τ. The relationship between τ and d is that one mean free path is equivelant to approximately 500 ft of air (at 20° C, 76 cm Hg). It should be pointed out that the curves of Fig. 2.1 are not simply plots of Eq. 2.1 for various values of d or τ. The theoretical curves of the figure include the effect of scattered radiation from the infinite-plane source which reaches the detector, whereas the equation accounts only for the uncollided radiation reaching the detector.

Nevertheless, it is possible to use a simple technique for predicting θ_{max} based on Eq. 2.1 The reason for this simplification is that the scattered part of the radiation does not contribute to rapid variations in dose with angle. To solve approximately for θ_{max} therefore, it is sufficient to equate to zero the derivative of Eq. 2.1 with respect to θ.

Then

$$\frac{\partial}{\partial\theta}\left[\frac{Se^{-\tau/\cos\theta}}{4\pi\cos\theta}\right] = 0$$

The solution to this equation is

$$\cos\theta_{max} = \tau$$

This simple approximate result shows that the cosine of the angle which corresponds to maximum dose is equal to the equivalent depth of the plane source in mean free paths.

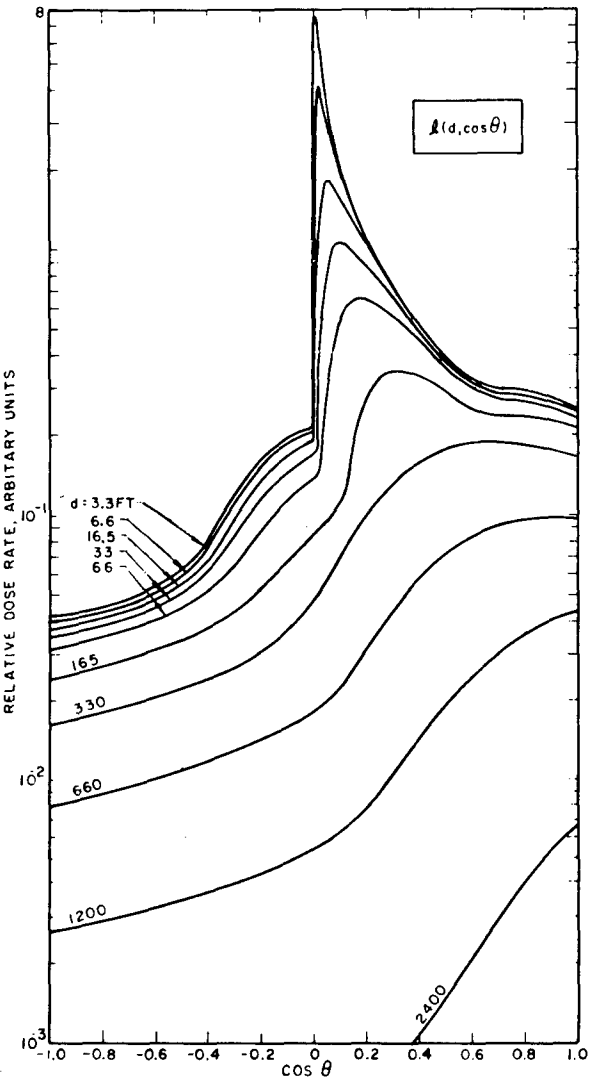

Fig. 2.1 – Variation of dose with angle and height above a plane (Spencer[1]).

2.4 ALTERNATE METHOD FOR DETERMINING EQUIVALENT DEPTH

In Sec. 2.3 it was shown that τ is a measure of ground roughness, in the sense that τ measures the equivalent number of mean free paths of scattering and absorbing material between the source and the detector. In this section alternate methods for determining τ are investigated. More properly, an attempt is made to determine ρ, which is the number of feet of air-equivalent distance that should be attributed to ground-roughness effects[2]. The units of ρ are the same as the units of d of Fig. 2.1.

In the case where fallout is distributed uniformly over a smooth infinite plane, let a detector be at a distance d above the plane. The intensity of the angular distribution of dose for several values of d is shown in Fig. 2.1. The angle θ represents the orientation of a directional detector and is the angle between the direction of the radiation being detected and a normal from the detector to the contaminated plane. That is, $\theta = 0$ when the detector is looking straight

down, $\theta = 90°$ when the detector is looking at the horizon, and $\theta = 180°$ when the detector is looking straight up.

It should be noted that the curves for ℓ (d, cos θ) of Fig. 2.1 were calculated for the gamma-ray spectrum of fission products 1.12 hr after the fission event and for an infinite medium of water.

The gamma-ray spectra were actually measured at 28, 40, and 131 hrs after fission. Dr. Spencer calculated the angular distributions of dose at the appropriate times for the present experiment[2]. Although there was very little difference between the curves for the various times involved, the theoretical curves corresponding to the times of the experimental measurements were used for comparison between theory and experiment.

The normalization of ℓ(d, cos θ) is such that

$$D_o = D(3) = \int_o^{\pi} \ell(3, \cos\theta) \sin\theta \, d\theta = 1$$

That is, the total dose at 3 ft above the surface is taken to be unity.

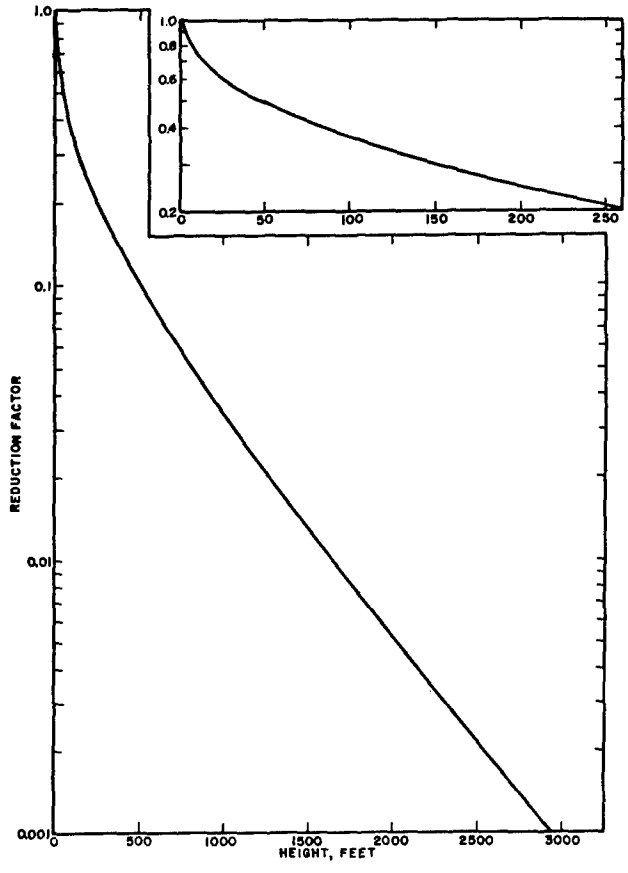

Fig. 2.2 – Variation of dose with height (Spencer[1]).

The variation of dose with height is given by

$$D/D_o = L(d)$$

Fig. 2.2 shows how L(d) varies with d.

In the case where there is a ground-roughness effect that makes the apparent distance from the hypothetical plane source to the detector greater than the actual height of the detector above the ground,

$$D/D_o = L(d + \rho)$$

where ρ is a parameter which gives some measure of ground roughness. In particular, ρ is the number of feet of air-equivalent distance attributed to the shielding effects of surface irregularities. The same parameter can be expected to apply for the case of angular distribution; that is, the expression

$$\ell(d + \rho, \cos \theta)$$

should be used to predict the angular distribution of radiation intensity at a distance d above a rough surface.

2.5 FALLOUT CONTOURS

Appendix A gives a treatment of expected fallout contours. It was necessary to make some rough predictions regarding the deposition of fallout so that appropriate areas in the vicinity of ground zero (GZ) could be thoroughly explored before D-Day and so that suitable areas could be plowed before the test.

REFERENCES

1. L. V. Spencer, *Structure Shielding Against Fallout Radiation from Nuclear Weapons*, NBS Monograph 42, 1962.

2. L. V. Spencer, Private Communication to C. M. Huddleston.

Chapter 3

EXPERIMENTAL ARRANGEMENT

3.1 GAMMA-RAY DETECTOR

The principal detecting device consisted of a Harshaw integral line assembly (type 12S) with a NaI(T1) crystal 3 in. in diameter by 3 in. high and a selected 3 in. Dumont 6363 photomultiplier tube. The resolution of the assembly was approximately 8% for the Cs^{137} 662-kev gamma-ray line.

Pulses from the phototube were fed through a 90-ft, 50-ohm cable (RG-58-U) into a Nuclear Data model 130A 512-channel pulse-height analyzer. The data were typed or recorded on punched tape.

Ionization chambers were used for local surveying and for dose-vs-height measurements.

3.2 COLLIMATOR

The detector assembly was housed in a cylindrical lead collimator designed and built by Edgerton, Germeshausen & Grier, Inc., Santa Barbara, California. The detector was shielded on all sides by 7 in. of lead. Sketches of the collimator are shown in Figs. 3.1 and 3.2 and a photograph of the completed shield assembly appears in Fig. 3.3.

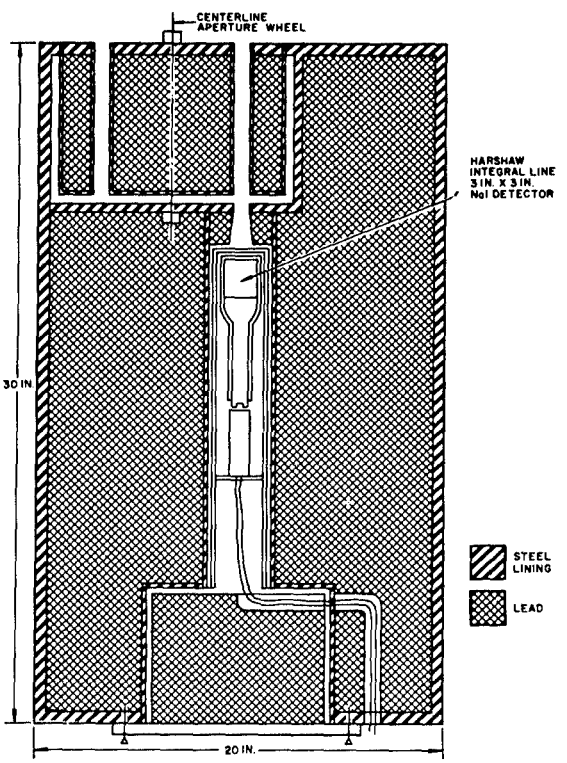

Fig. 3.1 – Cross-section sketch of shield (not to scale).

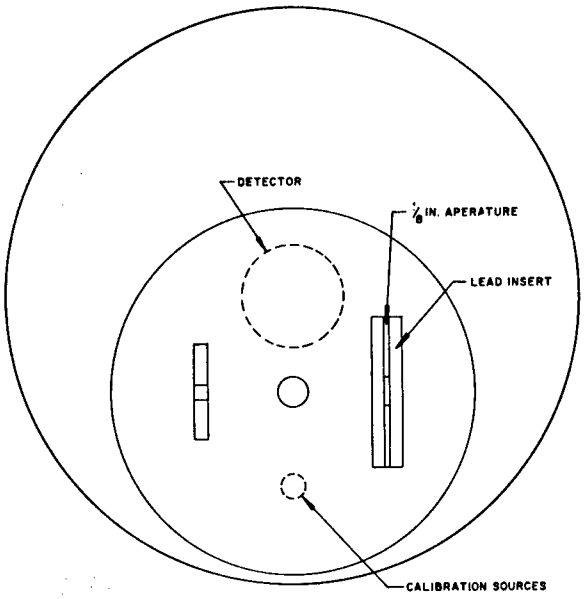

Fig. 3.2 – Top view of collimator showing rotating aperture wheel in closed position.

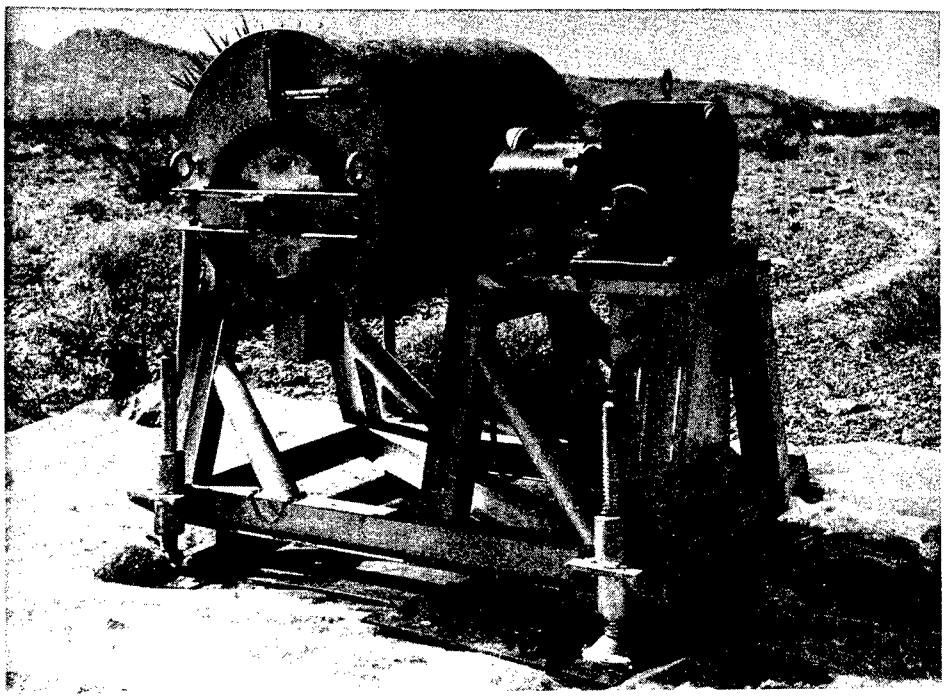

Fig. 3.3 – Complete shield assembly.

A power-driven rotating sub-unit allowed any of several apertures to be chosen. Figures 3.4 and 3.5 show the 0.50-inch x 20° wedge-shaped collimator aperture. There was also a 1.00-inch x 30° aperture which could be selected if the increase in counting rate justified the resultant loss in angular resolution. An insert was made to stop down the 1.00-inch x 30° aperture to a 0.50-inch cylindrical hole. Another insert provided for an aperture 1/8-in. by 30°. A third position was used for calibration with an internal Cs^{137}-Co^{60} source. In the fourth position, the detector was completely shielded for background measurements.

The unorthodox wedge-shaped aperature was chosen to increase the detector solid angle without an appreciable loss in angular resolution. This was possible because the differential dose was a sensitive function of polar angle but was not expected to be sharply dependent on azimuth. The geometry chosen (in the 0.50-inch by 20° case) allowed good resolution in angle (angle between the normal to the surface of the earth and the axis of the collimator aperture) and, at the same time, achieved a rather high solid angle (0.03 steradian).

The surface area of a smooth plane "seen" by the detector from a position 3 ft above the ground at various polar angles is shown in Fig. 3.6.

3.3 DOSE-VERSUS-HEIGHT MEASUREMENTS

Because of the importance of dose-vs-height measurements, as mentioned in Section 2.4, a vertical traverse was made of dose rate as a function of height above ground. An extension-ladder arrangement was used for this series of measurements.

3.4 THE MOBILE LABORATORY

A 5-ton Navy truck (borrowed from the U. S. Naval Civil Engineering Laboratory, Port Hueneme, California) was modified to serve as a mobile laboratory for work in the field. Photographs of the modified six-wheel-drive truck are shown in Figs. 3.7 and 3.8. Behind the cab was an Army electrical-equipment shelter measuring approximately 7 ft x 7 ft x 11 ft long. The inside walls of the shelter were covered with a 0.5-inch thickness of lead for personnel shielding. The interior of the shielded mobile laboratory with the shock-mounted laboratory instruments and air conditioner installed is shown in Figs. 3.9 and 3.10.

Behind the shielded shelter was a wooden enclosure for housing the collimator while in transit. A 2-ton hoist was used to raise and lower the collimator.

Power for equipment, lights, and air conditioning was supplied by a 5-kva gasoline-powered motor-generator set.

Figure 3.11 shows a typical experimental setup. The collimator was operated remotely from inside the personnel shelter on the truck, which was driven at least 50 ft from the collimator location before angular-distribution measurements were made.

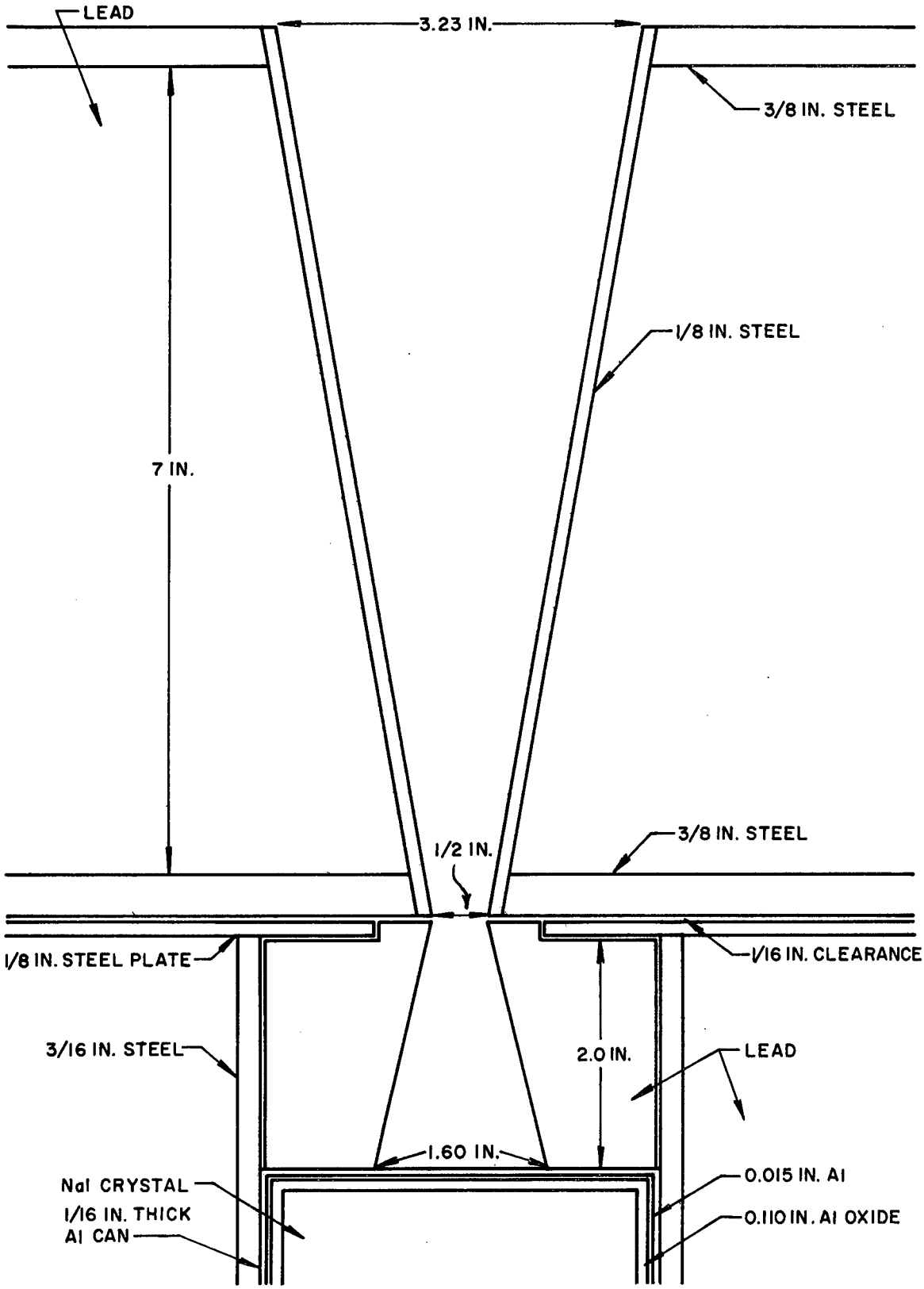

Fig. 3.4 – Wedge-shaped collimator aperture, horizontal cross section.

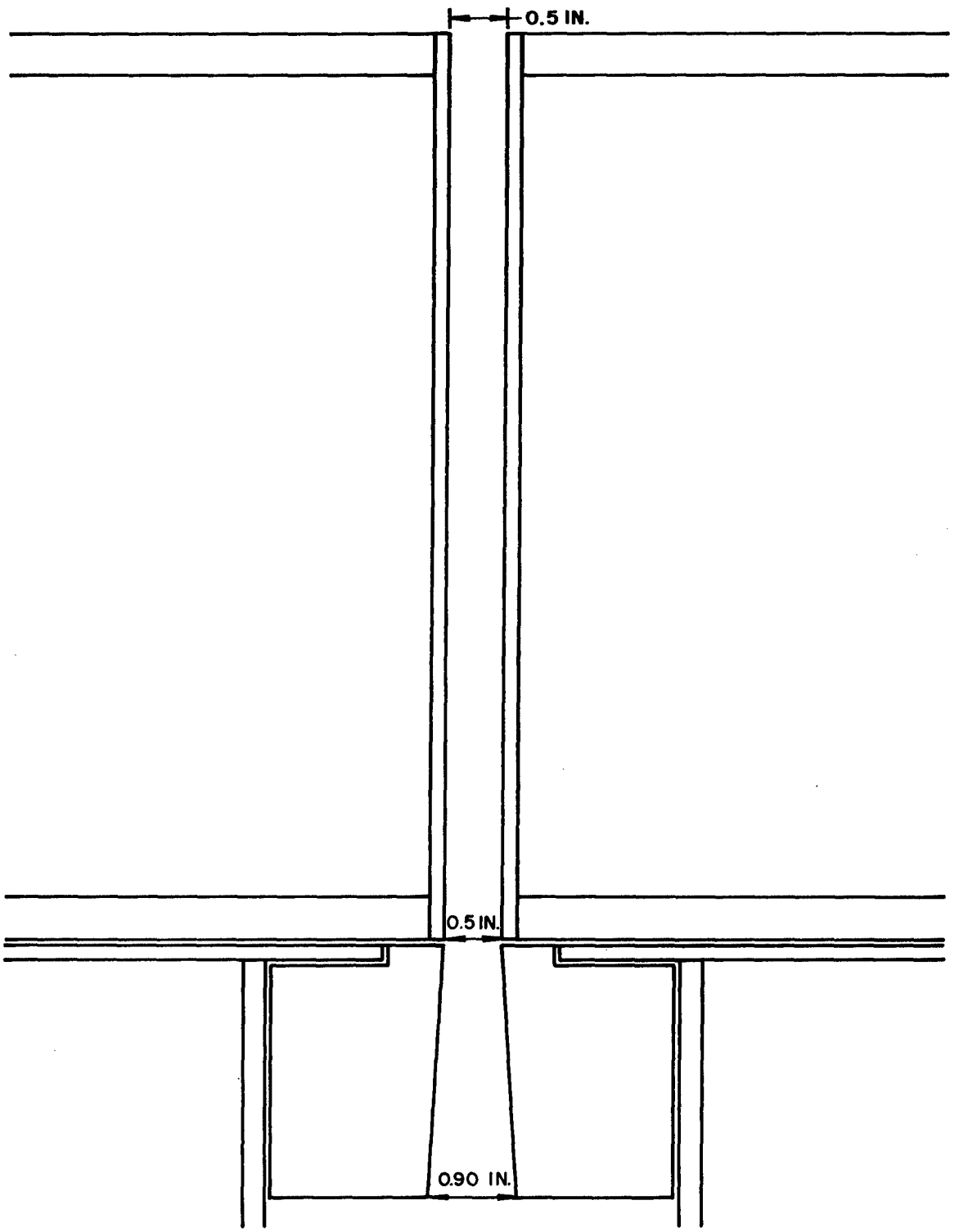

Fig. 3.5 – Wedge-shaped collimator aperture, vertical cross section.

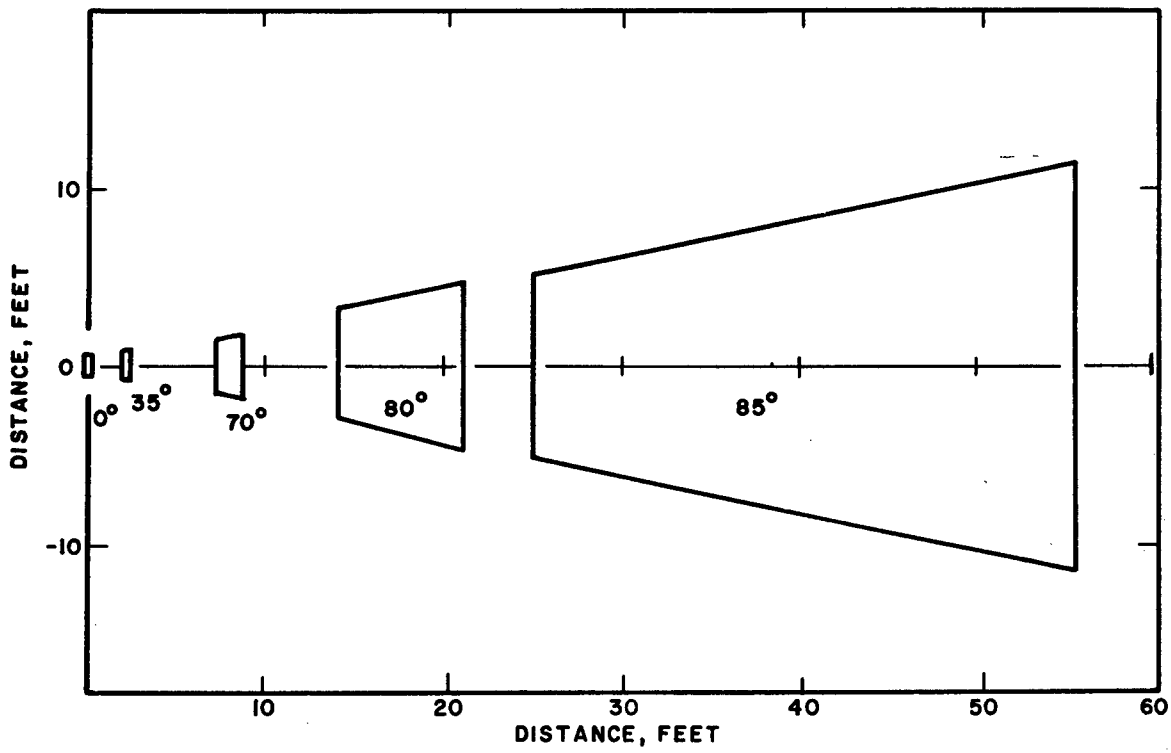

Fig. 3.6 – Area seen by 0.50-in. by 20° collimator aperture as a function of polar angle.

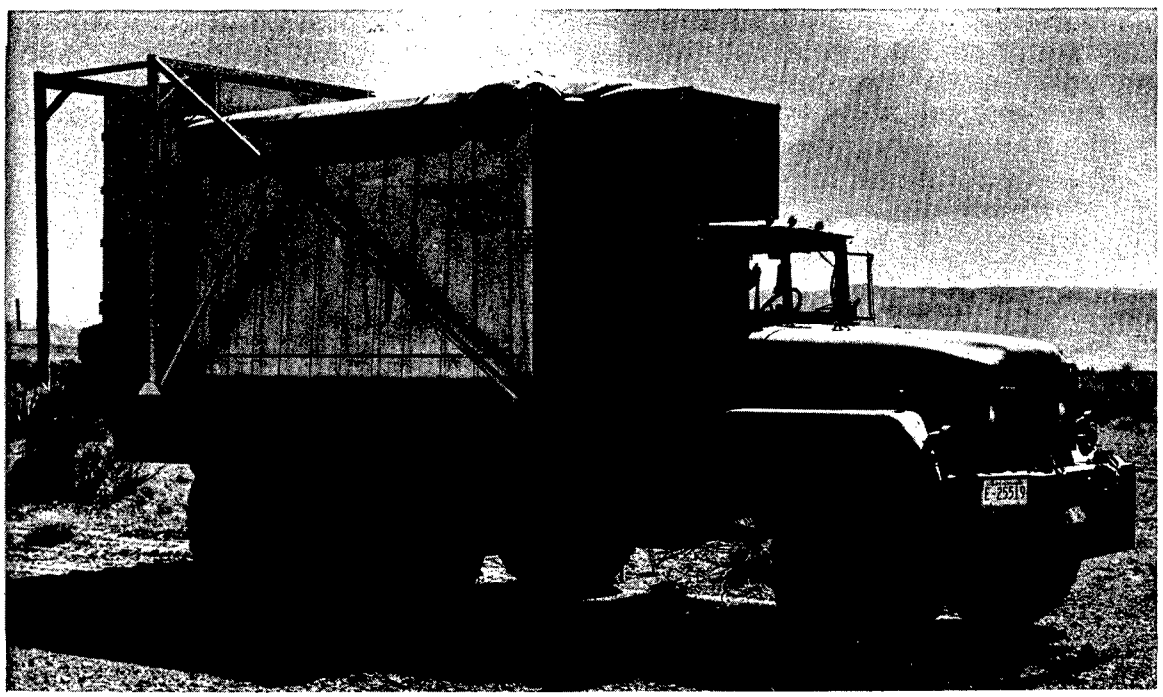

Fig. 3.7 – Six-wheel-drive truck

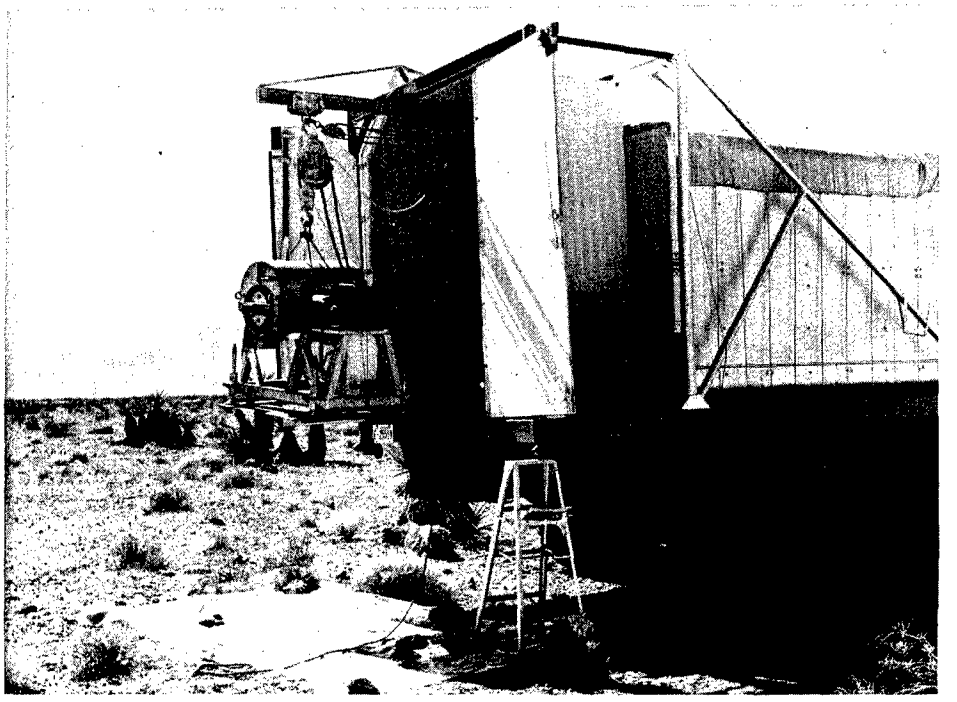

Fig. 3.8 – Shield assembly on six-wheel-drive truck.

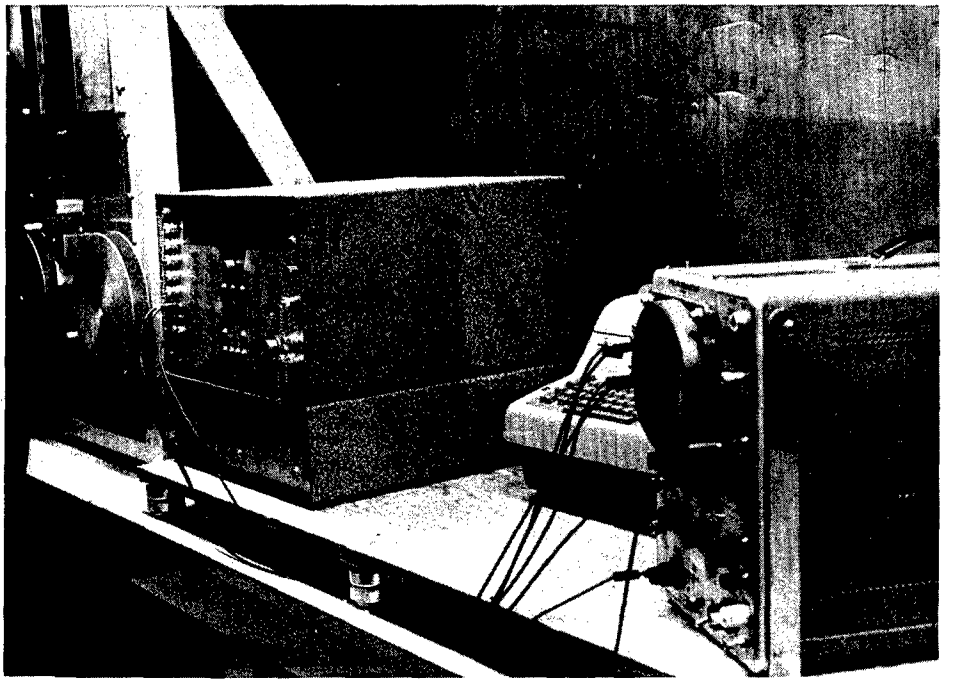

Fig. 3.9 – Shock-mounted instruments in shielded mobile laboratory.

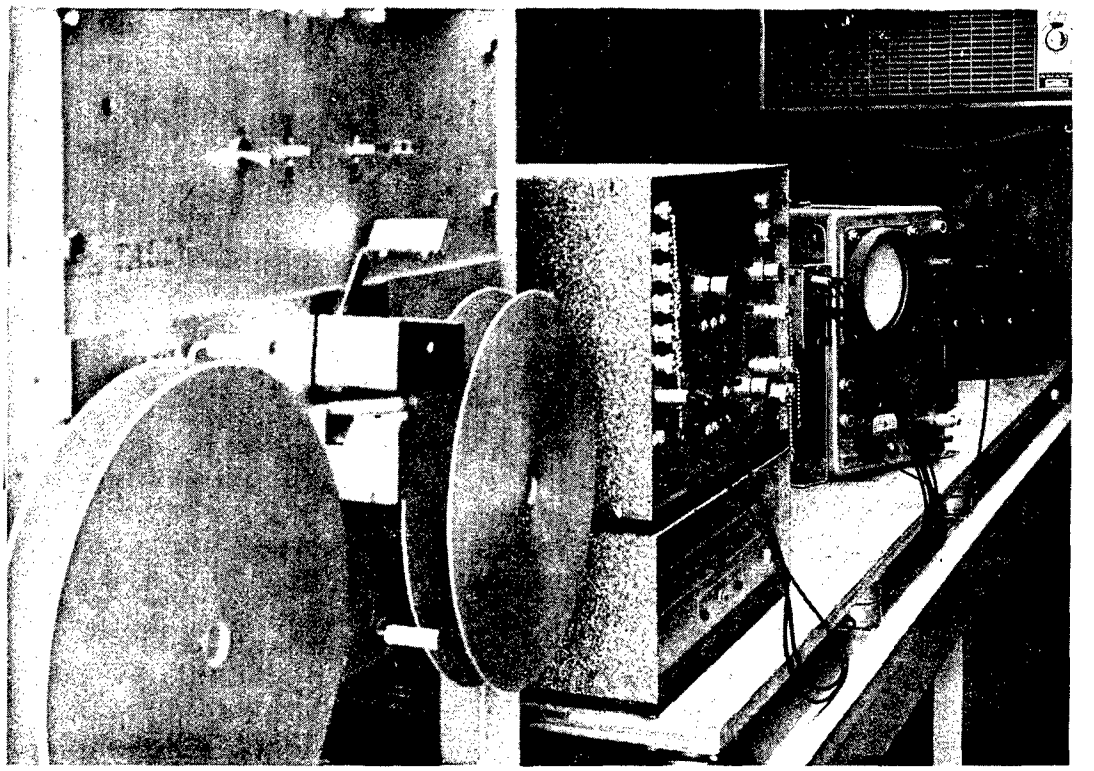

—●—

Fig. 3.10 – Laboratory instruments and air conditioner in shielded mobile.

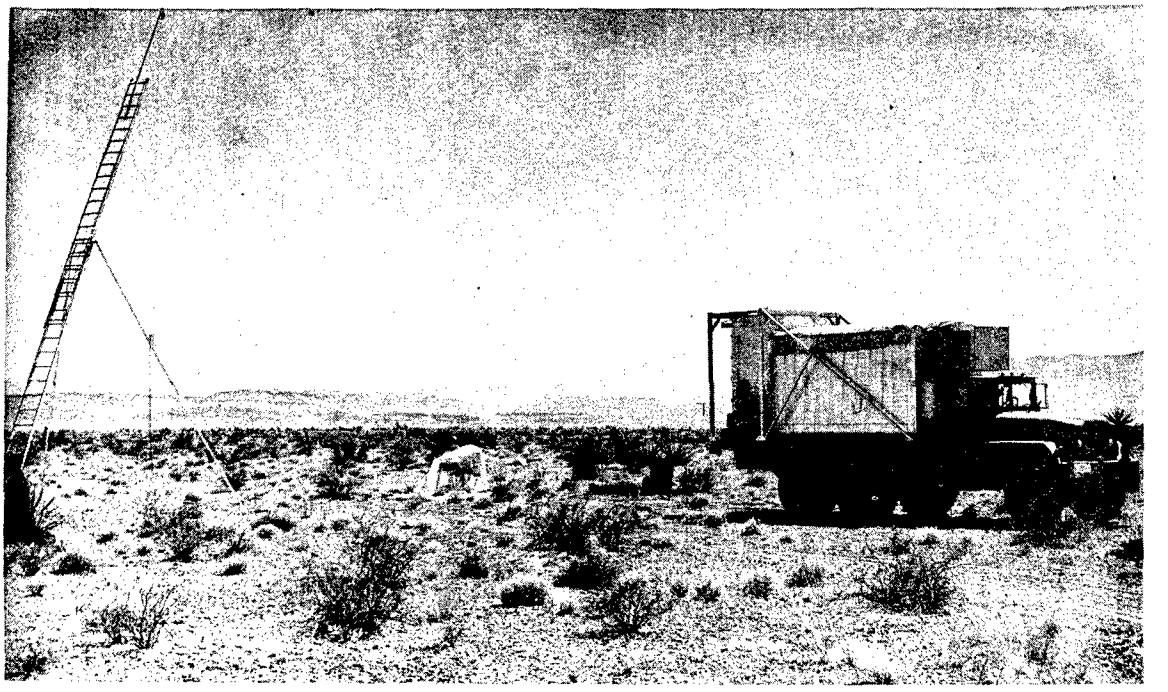

—●—

Fig. 3.11 – Typical experimental setup.

Chapter 4

FIELD OPERATIONS

One type of terrain needed to meet the objectives of the project was one with a known and controlled degree of roughness. Three areas were plowed several miles downwind in the predicted fallout path in hope that fallout would be deposited on at least one. Two of these fields were located in the dry-lake bed north of Indian Springs Air Force Base and the third in the dry-lake bed northeast of the base. Furrows about 6 in. deep were plowed every 30 in. Each field was square and about 1500 ft on a side.

The actual fallout path was about 20° north of east from Frenchman Flat. This path missed the dry-lake beds and plowed fields in the first valley north of Indian Springs. However, the plowed field and dry-lake beds in the second valley (about 30 miles from GZ) were near the center of the fallout pattern. The winds were rather slow, and the cloud was nearly dispersed by the time it reached the second valley. As a result, the dose rates were quite low.

Even though these dose rates were a factor of 10 lower than desirable, it was decided to obtain as much data as possible. Energy and angular-distribution measurements were made with the NaI crystal and collimator all day and evening on D + 1 day at both a dry-Lake bed and a plowed field. Long counts were necessary to obtain statistically valid data.

Dose-rate-vs-height and decay measurements were not successful at these two locations because of instrument problems, temperature effects, and low dose rates, even though several attempts were made on different days and nights.

Contamination appeared to be distributed quite uniformly over large areas at these two locations. Survey meter readings out to 1000 ft showed no detectable change in radiation level. In addition, aerial surveys [1] at 500 ft indicated that fallout was distributed uniformly over these areas.

Integrated doses at 3 ft were measured quite accurately by low-range ionization chambers and pocket ionization chambers with tin sleeves to improve the energy response.

Figures 4.1 and 4.2 show the area used for measurements at the dry-lake bed. The ground was hard and smooth with cracks every few inches. The cracks were, on the average, approximately 18 in. apart, 1 in. deep, and 1/4 in. wide. They formed irregular polygonal shapes on the lake-bed surface. Within the polygons there were other small surface irregularities, but deviations from a flat plane did not exceed 1/8-in.

Figures 4.3 to 4.5 show the plowed fields used for measurements. Figure 4.6 contains sketches of the collimator location in relation to the size of the field and shows the approximate size of the furrows and ridges. The furrows ran north and south, and the collimator pointed west.

On the evening of D + 5 day, measurements were made in the center of the fallout path about 8 miles from GZ over typical rough desert terrain. All instrumentation functioned properly and good data were taken. These data included: energy and angular distribution, dose rate as a function of height (1 to 40 ft), dose rate at 3 ft, and dose-rate-vs.-time (decay). Again there were no detectable changes in the dose rate within 1000 ft of the experimental setup.

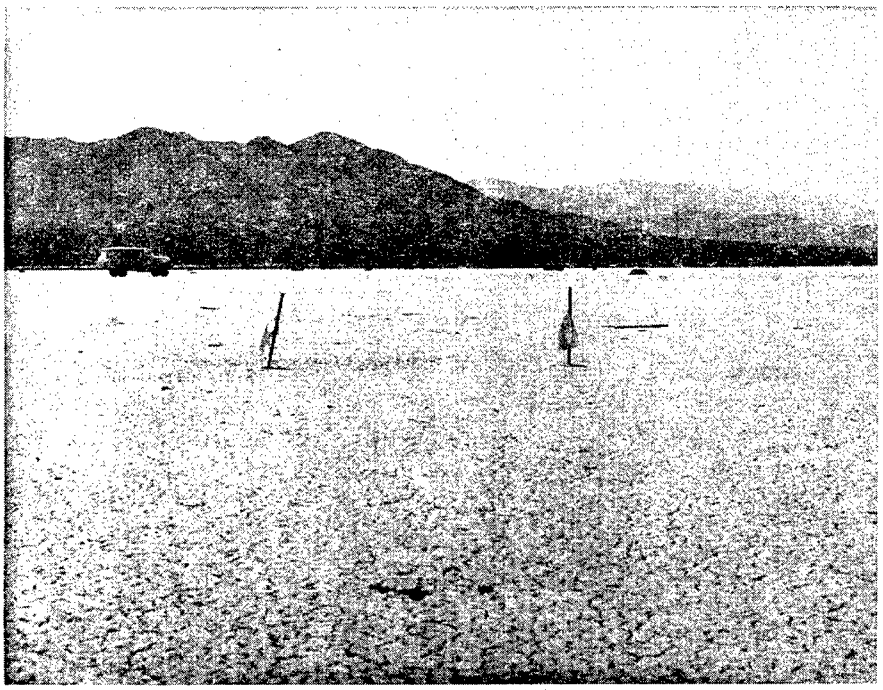

—●—

Fig. 4.1 – Experimental area at a flat dry-lake bed.

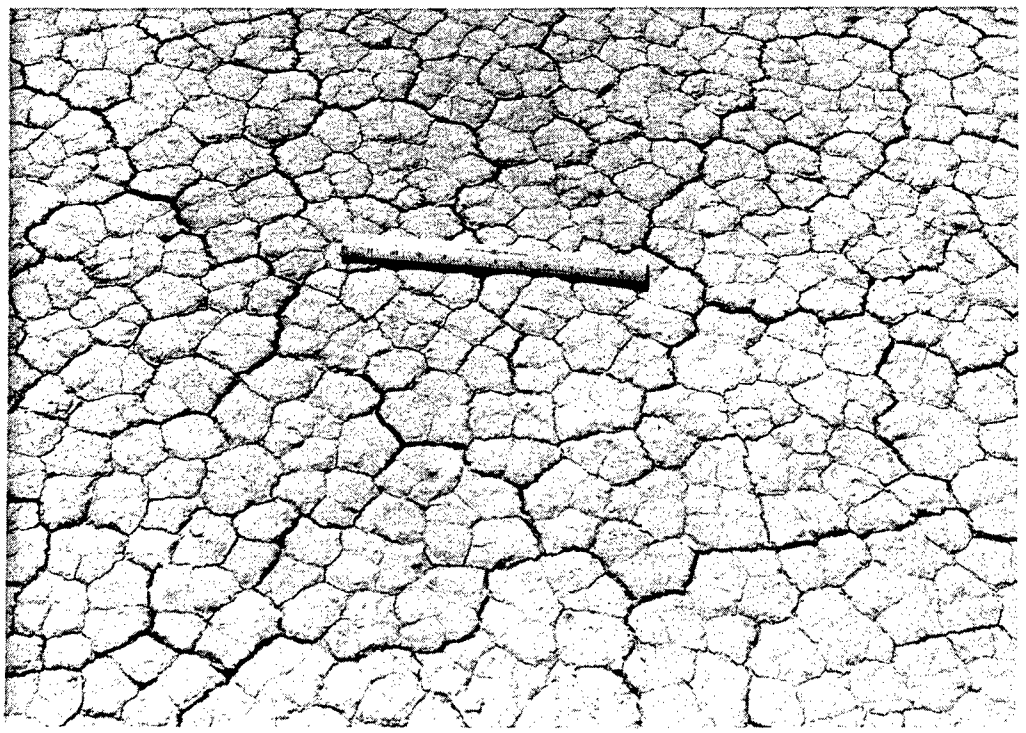

—●—

Fig. 4.2 – Close-up view of dry-lake bed.

—●—

Fig. 4.3 – Plowed field used for measurements.

—●—

Fig. 4.4 – Close-up view of plowed field.

Fig. 4.5 – Plowed field as seen by collimator.

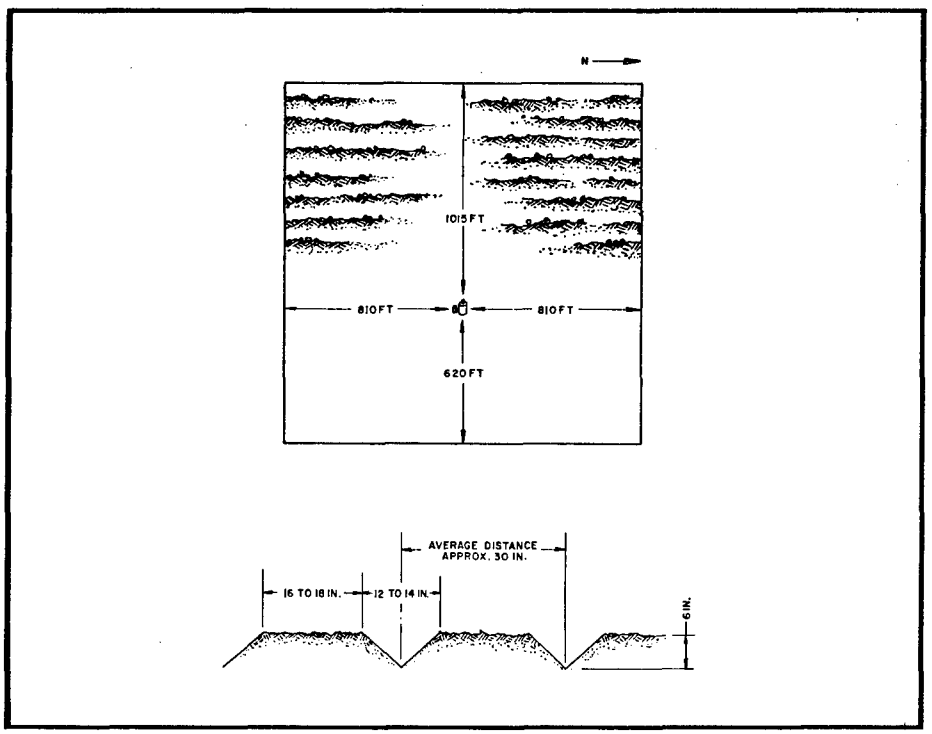

Fig. 4.6 – Profile of ground surface, plowed field.

Figures 4.7 to 4.9 are photographs of typical terrain at the measurement location.

Several profile surveys were made using a transit to determine locations of washes and ridges in the vicinity of the measurement area. Figure 4.10 is a graph showing the slope of the ground and terrain features in the direction the collimator was pointing*. Figures 4.11 to 4.14 show profile surveys at dose-vs-height measurement locations.

Figure 4.15 shows estimated shadowed areas in the 20° sector toward which the collimator was pointing. These shadowed areas represent areas on the ground not "seen" from the collimator location 3 ft above the ground.

Unfortunately, limited time and personnel available for measurements in the field did not permit a sampling program to determine source strengths at the three positions where angular distributions were made.

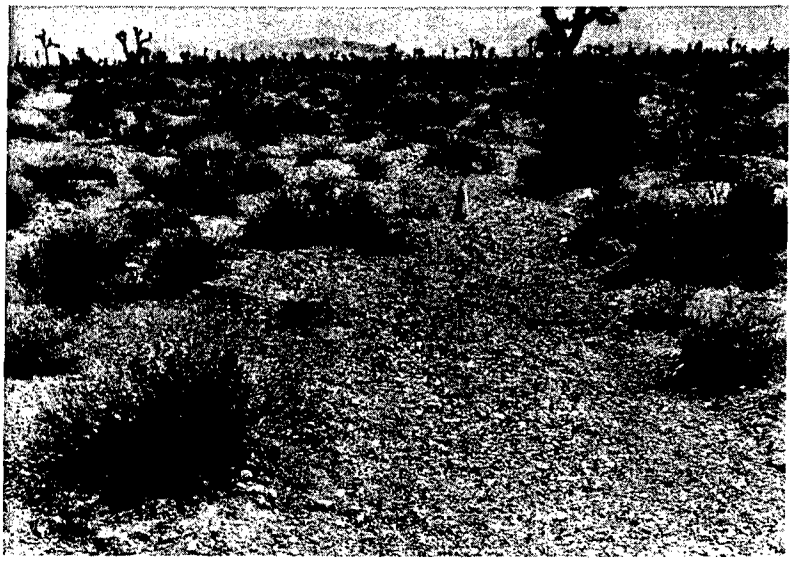

—●—

Fig. 4.7—
Typical desert terrain.

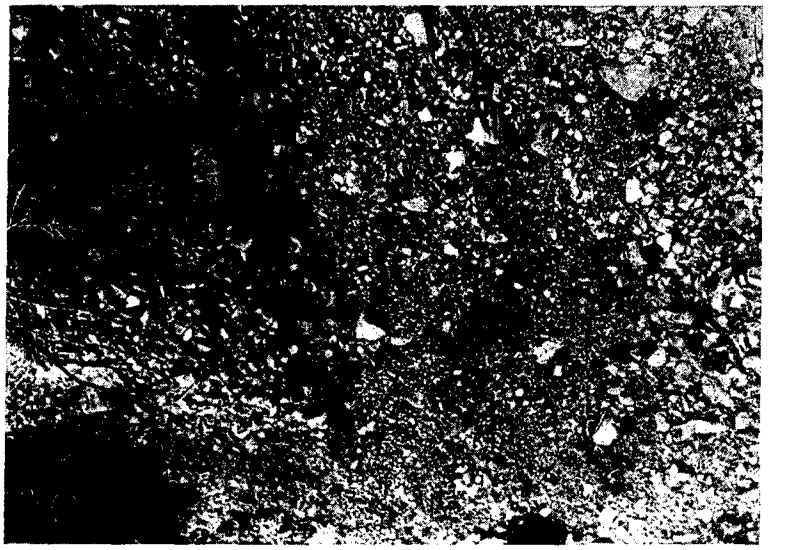

—●—

Fig. 4.8 —
Brush and rocks in desert terrain.

*Since the surface was not horizontal at this location, the data have been corrected for the 2° slope.

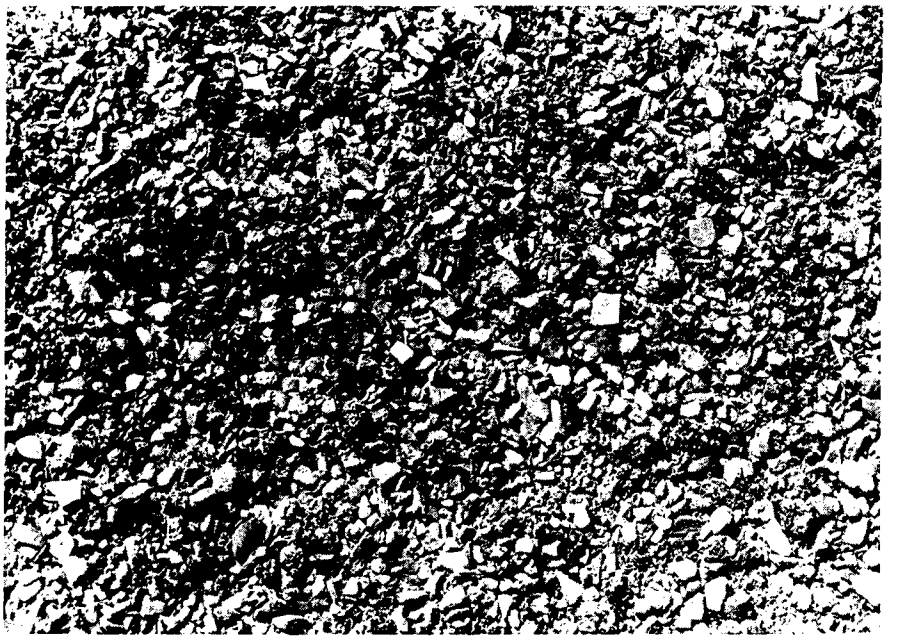

Fig. 4.9 – Close-up view of desert terrain. Area shown is roughly 4 sq. ft.

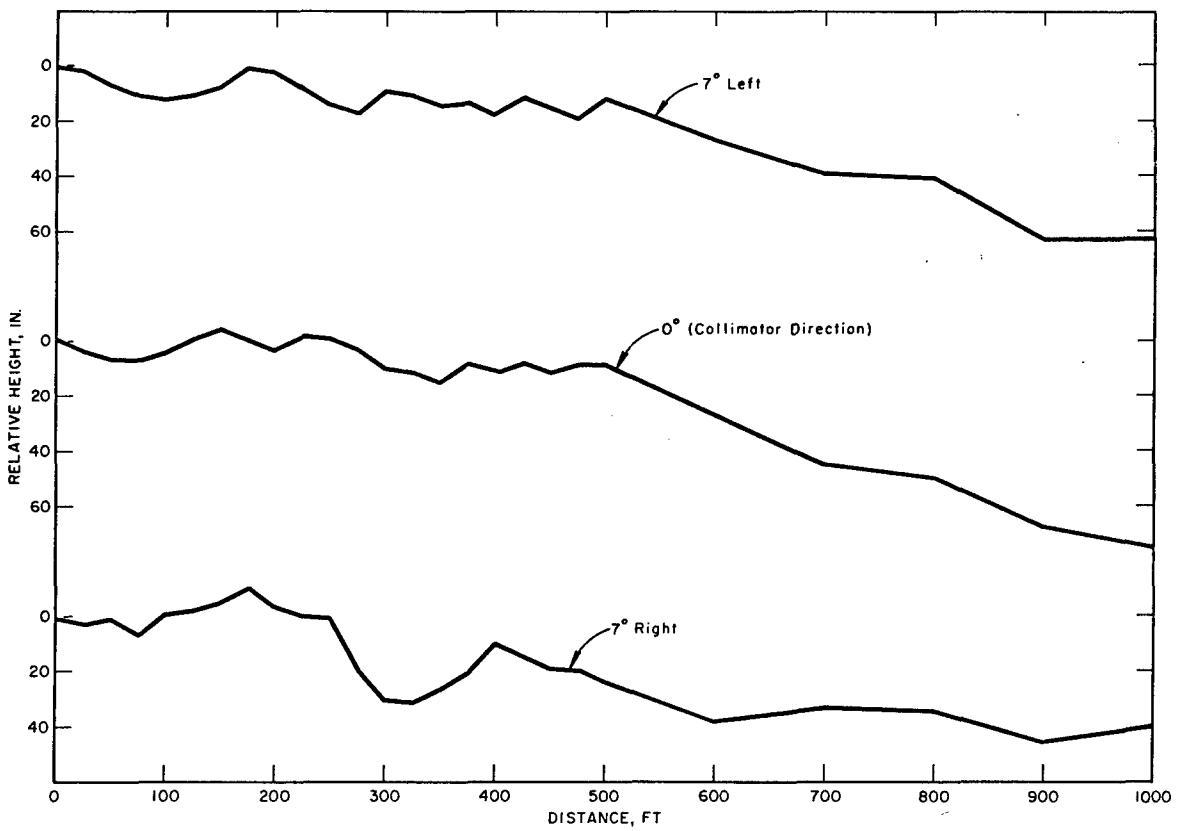

Fig. 4.10 – Profile of terrain in the plane of the collimator.

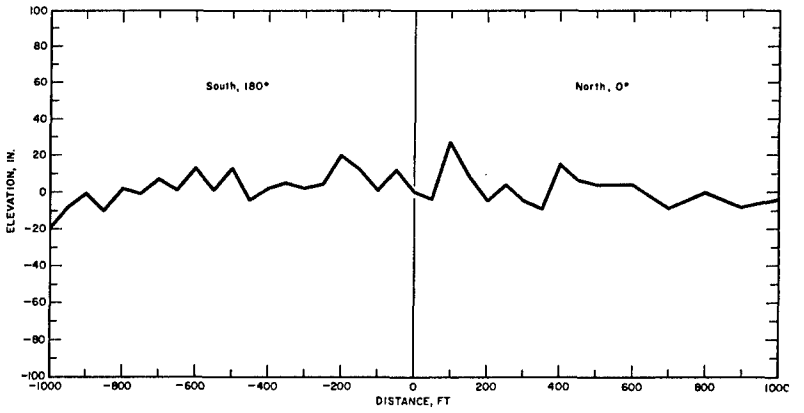

Figure 4.11 –
Profile of terrain from location of dose-vs-height measurements.

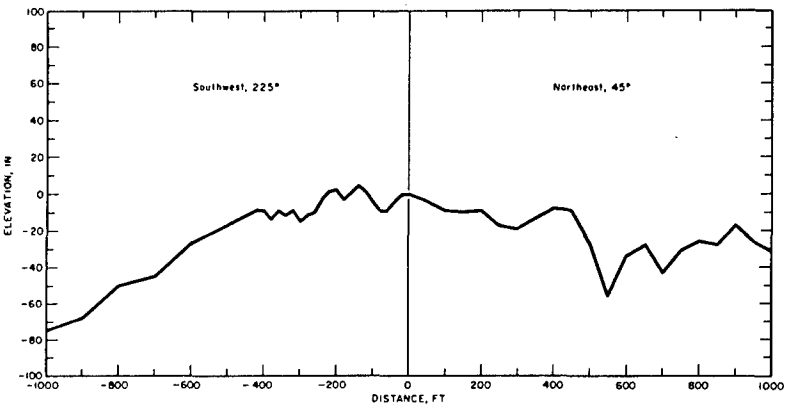

Figure 4.12 –
Profile of terrain from location of dose-vs-height measurements.

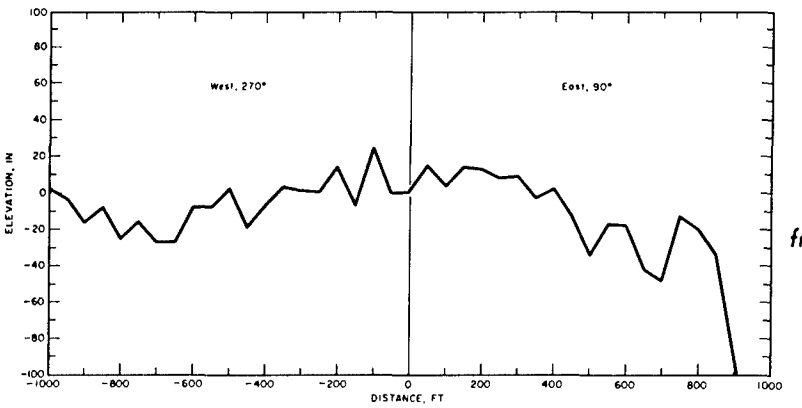

Fig. 4.13 –
Profile of terrain from location of dose-vs-height measurements

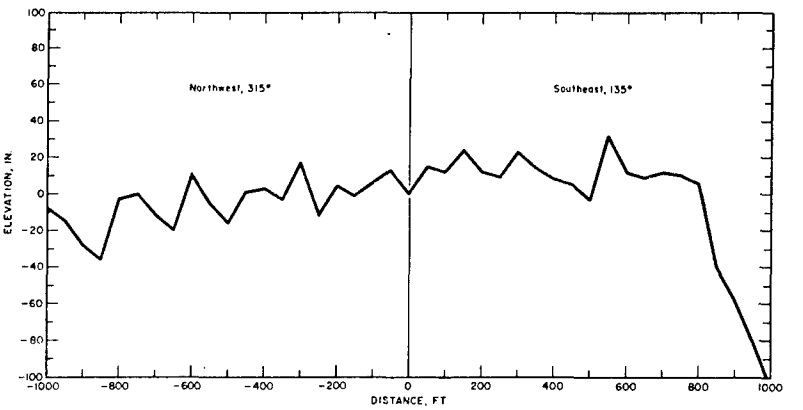

Fig. 4.14 –
Profile of terrain from location of dose-vs-height measurements.

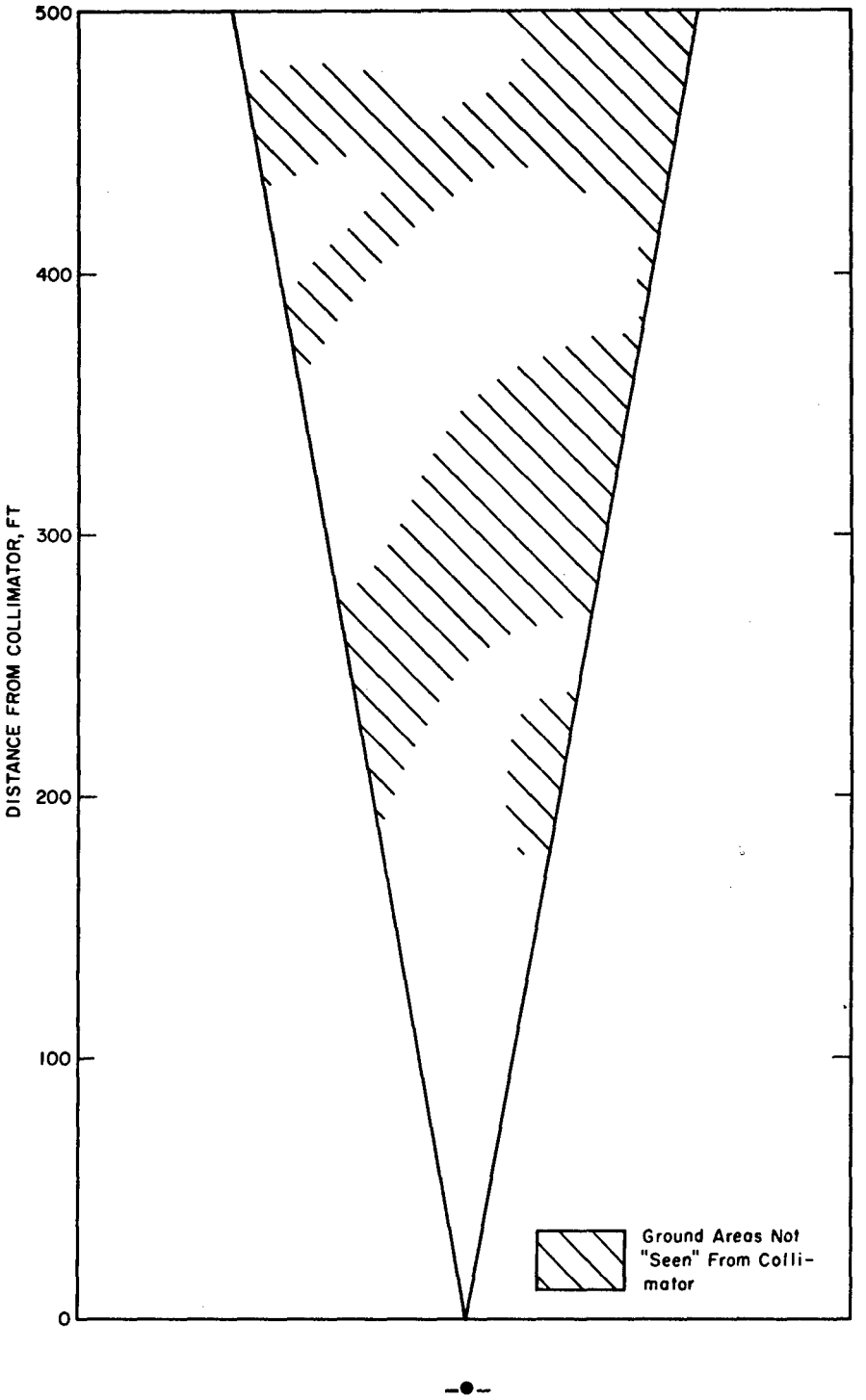

Fig. 4.15 – Ground areas not seen by collimator at rough desert terrain.

REFERENCES

1. Robert Guillou, EG&G Santa Barbara Laboratory, Private Communication.

Chapter 5

RESULTS

5.1 DOSE-VERSUS-HEIGHT MEASUREMENTS

The dose-vs-height measurements over the dry-lake bed and over the plowed field were not successful because of instrument instability. Although several attempts were made to obtain good data for the variation of dose with height, the extreme heat of the Nevada desert in mid-summer caused unpredictable and non-repeatable variations in successive sets of measurements. It was with great reluctance that the experimenters, after repeated unsuccessful tries, decided to abandon attempts to obtain dose-vs-height data for two of the three types of terrain investigated.

Above the third position, typical wild desert terrain, dose-vs-height measurements appeared to be valid. Figure 3.11 shows the ladder used to raise the detector from 1 to 40 ft above the ground. A Nuclear Chicago Cutie Pie integrating ionization Chamber (Model No. 2588 with Model No. 2526 chamber) was used as a detector. The slight anisotropy of this detector is discussed in Section 6.1. Two series of measurements were made: the first at H + 127.8 hours, and the second at H + 128.1 hours. Each series of measurements required approximately 5 min. Table 5.1 lists the experimental results.

Since the two runs were taken close together in time, no decay correction is used in comparing them. Figure 5.1 shows the experimental points for dose measurements above the site of the typical desert terrain. The solid curve is a normalized plot of $L(d+\rho)$ for $\rho = 40$ ft as described in Section 2.4. It is seen that the two experimental measurements agree well with each other and that the data are fit well by a theoretical curve having the shape of $L(d + 40)$. This agreement was taken as evidence to support the theory outlined in Section 2.4. Moreover, it appeared that the ground-roughness effect of the site chosen was comparable to an equivalent additional distance of 40 ft from ground to detector.

TABLE 5.1
DOSE-VS-HEIGHT DISTRIBUTION AT ROUGH DESERT LOCATION

HEIGHT (ft)	DOSE RATE, mr/25 sec	
	FIRST MEASUREMENT	SECOND MEASUREMENT
1	0.227	0.226
2	0.230	0.226
3	0.227	0.227
4	0.225	0.225
5	0.226	0.222
7	0.223	0.219
10	0.216	0.216
15	0.212	0.209
20	0.206	0.200
25	0.200	0.194
30	0.191	0.190
35	0.185	0.185
38.5	0.182	0.181

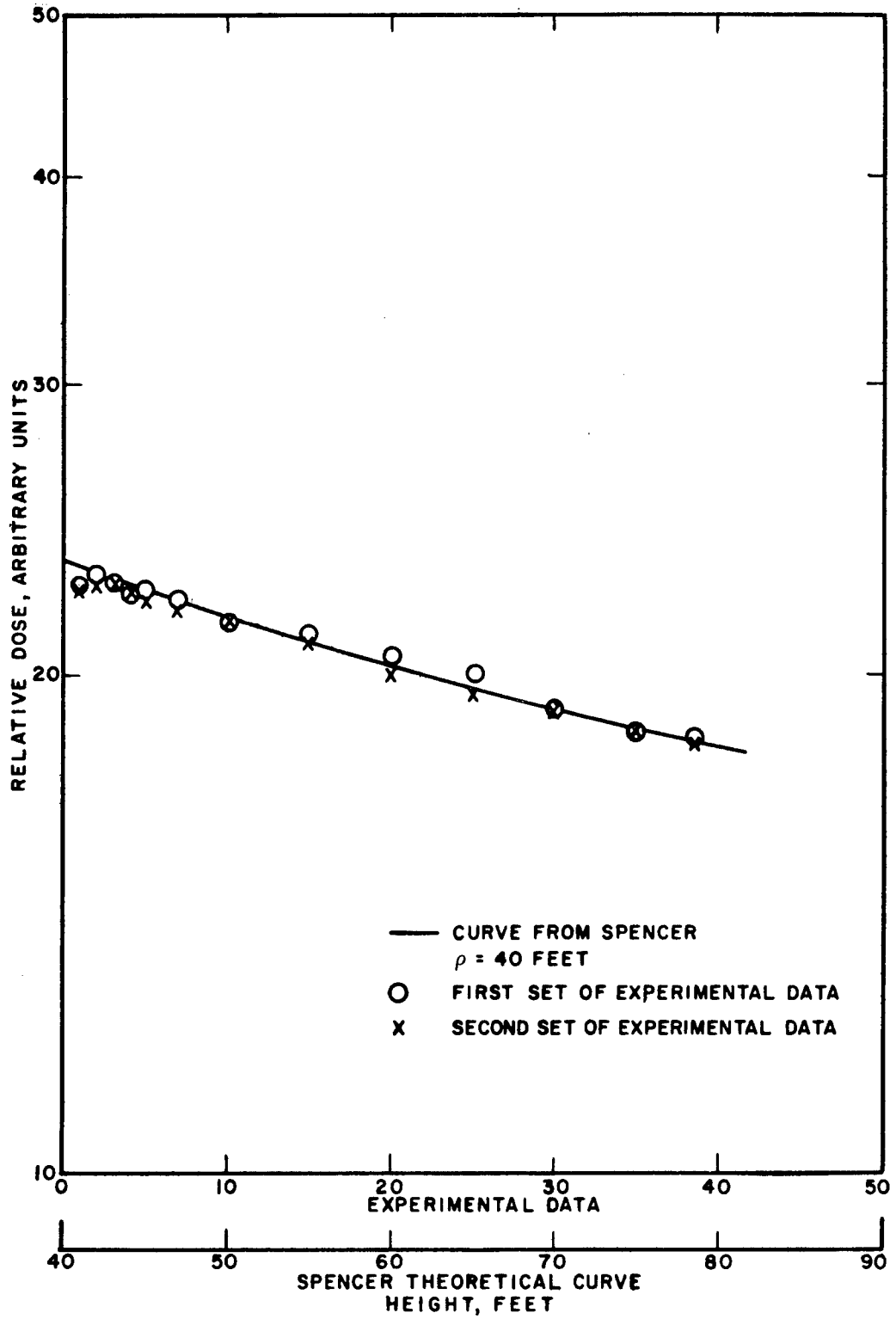

Fig. 5.1 – Dose-vs-height above typical desert terrain.

5.2 MEASUREMENTS OVER DRY-LAKE BED

On the morning of the day after detonation, the experimental crew of six men proceeded in two vehicles into East Indian Springs Valley. The first vehicle, a 4-wheel-drive carryall, went ahead of the mobile laboratory to monitor the radiation field and find a suitable area for measurements. A satisfactory area was found approximately 30 miles east-northeast of GZ on a flat dry-lake bed. The radiation field appeared to be quite uniform for over 1000 ft in all directions from the measurement site chosen. It was a hot, clear day with a few small, scattered clouds near the horizon. There was a light southerly wind; visibility was excellent; barometric pressure was 26.55 in. of Hg.

The collimator was lowered to the ground, and the truck was driven about 50 ft west. The collimator pointed, when it was looking at the horizon, approximately east-southeast. The lake bed (or playa) extended about 2500 ft in that direction from the collimator. Spectrum measurements were begun very nearly at H + 24 hr.

Two local radiation surveys were made. A man walked out 1,000 ft in the direction the collimator pointed, calling out readings of a survey meter every 100 ft. The readings of the meter, which was held 3 ft above ground, are given in Table 5.2.

A troublesome difficulty arose from the shifting gain of the detector. Presumably, this gain shift was caused by the gradual heating of the massive lead collimator. Although the collimator was sprayed with aluminum enamel to minimize the absorption of solar radiation, there was no mechanism to hold the temperature constant at the detector. The gain of the analyzer was adjusted at the beginning of each spectrum measurement. Corrections were subsequently made for gain shift during analysis, as will be discussed in Section 6.2.2.

Some sample data are displayed in Table 5.3. For all cases the live time of the analyzer was 8 min. The data shown were gathered at times between H + 24 and H + 30 hr. Counts were taken in 256 channels, each 10-kev wide. Results are shown only for the first 168 channels, however, because there were essentially no counts (above background) in the channels higher than 168. Data are exhibited for 0° (looking straight down), 180° (looking straight up), and 85° (just below the horizon, the collimator elevation for maximum counting rate). The collimator aperture used was 1/2 in by 20°.

Table 5.3 shows that there are some spurious high-background counts in some of the low-energy channels for the 180° case. These high counts in low channels were attributed to noise from the selsyn motor which was used as a remote indicator to measure the elevation angle of the collimator. For data analysis, the most obviously spurious counts were replaced by interpolated counting rates.

TABLE 5.2
RADIATION SURVEY AT DRY-LAKE BED

DISTANCE FROM COLLIMATOR, ft	DOSE RATE, mr/hr FIRST RUN	DOSE RATE, mr/hr SECOND RUN
100	3.5	3.5
200	3.5	3.5
300	3.5	3.5
400	3.5	3.5
500	3.5	3.0
600	4.0	3.0
700	3.5	3.5
800	3.5	3.0
900	3.5	3.5
1000	3.5	3.0

TABLE 5.3
COUNTING RATE PER ANALYZER CHANNEL AT DRY LAKEBED

CHANNEL NO.	ELEVATION 0		ELEVATION 85		ELEVATION 180	
	DATA	BKGD.	DATA	BKGD.	DATA	BKGD.
1	0.	0.	1.	0.	2.	3.
2	16.	5.	30.	8.	39.	42.
3	82.	39.	167.	48.	120.	836.
4	176.	58.	373.	73.	197.	503.
5	176.	49.	402.	57.	275.	54.
6	180.	80.	446.	109.	412.	91.
7	276.	117.	564.	144.	507.	113.
8	290.	110.	565.	107.	492.	100.
9	359.	79.	671.	92.	461.	81.
10	342.	53.	644.	57.	464.	63.
11	332.	51.	652.	43.	354.	44.
12	353.	45.	660.	52.	311.	56.
13	327.	61.	587.	57.	286.	58.
14	335.	57.	844.	46.	266.	60.
15	360.	54.	979.	55.	243.	65.
16	295.	46.	730.	41.	235.	63.
17	247.	54.	513.	44.	215.	51.
18	230.	53.	554.	52.	213.	49.
19	229.	64.	513.	56.	195.	58.
20	246.	55.	501.	58.	192.	53.
21	220.	63.	519.	62.	175.	63.
22	226.	65.	534.	69.	175.	51.
23	234.	53.	648.	37.	136.	55.
24	260.	44.	628.	54.	147.	47.
25	186.	46.	562.	42.	115.	58.
26	158.	36.	497.	49.	114.	34.
27	172.	47.	475.	37.	110.	40.
28	184.	33.	491.	46.	98.	33.
29	152.	36.	545.	33.	84.	34.
30	159.	31.	550.	39.	71.	28.
31	147.	44.	472.	38.	78.	27.
32	129.	35.	487.	35.	63.	32.
33	114.	35.	431.	34.	49.	28.
34	118.	31.	391.	28.	44.	26.
35	132.	42.	365.	26.	51.	34.
36	92.	27.	361.	35.	46.	35.
37	94.	24.	336.	32.	44.	34.
38	80.	23.	251.	25.	45.	35.
39	71.	22.	245.	22.	40.	27.
40	74.	32.	260.	22.	30.	18.
41.	52.	29.	268.	28.	35.	16.
42	61.	27.	238.	28.	30.	35.
43	65.	26.	278.	24.	34.	28.
44	59.	22.	236.	24.	36.	22.
45	71.	18.	252.	33.	38.	22.
46	75.	28.	274.	26.	41.	16.
47	78.	35.	277.	22.	21.	16.
48	85.	22.	317.	18.	36.	29.
49	99.	22.	395.	27.	25.	21.
50	110.	33.	434.	21.	25.	31.
51	104.	20.	528.	23.	29.	14.
52	111.	17.	591.	20.	34.	25.
53	82.	17.	468.	11.	21.	15.
54	67.	18.	425.	13.	36.	21.
55	71.	20.	320.	15.	17.	19.
56	41.	14.	241.	12.	22.	11.

TABLE 5.3 (Continued)
COUNTING RATE PER ANALYZER CHANNEL AT DRY LAKEBED

CHANNEL NO.	ELEVATION 0		ELEVATION 85		ELEVATION 180	
	DATA	BKGD.	DATA	BKGD.	DATA	BKGD.
57	60.	13.	205.	15.	24.	16.
58	52.	14.	216.	20.	22.	17.
59	50.	17.	222.	16.	20.	16.
60	68.	13.	258.	24.	22.	12.
61	96.	15.	348.	14.	24.	15.
62	108.	13.	494.	21.	22.	20.
63	111.	10.	555.	18.	25.	15.
64	112.	15.	662.	10.	20.	14.
65	94.	14.	617.	16.	23.	16.
66	62.	6.	513.	14.	25.	10.
67	81.	12.	427.	7.	22.	15.
68.	62.	10.	366.	9.	19.	10.
69	69.	9.	326.	15.	13.	12.
70	93.	7.	404.	15.	19.	18.
71	109.	7.	478.	14.	21.	16.
72	87.	10.	476.	16.	24.	6.
73	73.	11.	482.	14.	16.	15.
74	66.	11.	444.	12.	14.	18.
75	55.	18.	328.	12.	15.	10.
76	47.	12.	280.	4.	13.	12.
77	37.	9.	180.	10.	17.	11.
78	38.	10.	140.	11.	20.	9.
79	30.	10.	113.	4.	18.	9.
80	32.	12.	106.	11.	18.	14.
81	32.	14.	75.	12.	16.	10.
82	18.	10.	82.	9.	14.	6.
83	23.	15.	74.	5.	15.	8.
84	29.	8.	66.	10.	19.	7.
85	24.	8.	69.	8.	14.	9.
86	25.	6.	72.	6.	12.	7.
87	16.	7.	58.	11.	15.	11.
88	11.	9.	62.	7.	15.	10.
89	15.	2.	70.	15.	15.	9.
90	23.	9.	71.	11.	14.	6.
91	21.	6.	61.	7.	8.	4.
92	21.	7.	52.	5.	9.	5.
93	21.	3.	71.	7.	15.	11.
94	15.	5.	50.	5.	6.	8.
95	21.	11.	53.	4.	11.	4.
96	20.	7.	49.	13.	14.	3.
97	11.	8.	55.	10.	12.	10.
98	23.	7.	69.	6.	10.	6.
99	20.	12.	68.	6.	9.	7.
100	13.	3.	46.	6.	9.	7.
101	23.	7.	44.	10.	8.	8.
102	11.	11.	39.	6.	14.	9.
103	15.	8.	37.	10.	17.	10.
104	16.	5.	38.	2.	9.	8.
105	13.	3.	28.	2.	15.	4.
106	7.	11.	36.	5.	8.	3.
107	8.	6.	40.	8.	11.	9.
108	15.	5.	47.	4.	7.	7.
109	16.	5.	49.	3.	13.	7.
110	15.	10.	41.	6.	10.	11.
111	16.	4.	34.	9.	9.	5.
112	13.	3.	38.	6.	13.	5.

TABLE 5.3 (Continued)
COUNTING RATE PER ANALYZER CHANNEL AT DRY LAKEBED

CHANNEL NO.	ELEVATION 0		ELEVATION 85		ELEVATION 180	
	DATA	BKGD.	DATA	BKGD.	DATA	BKGD.
113	12.	3.	42.	6.	11.	7.
114	6.	4.	32.	10.	10.	6.
115	17.	7.	26.	8.	6.	2.
116	10.	8.	39.	9.	7.	5.
117	15.	10.	25.	8.	9.	5.
118	11.	5.	27.	3.	7.	6.
119	15.	6.	27.	5.	8.	3.
120	6.	4.	36.	4.	9.	4.
121	11.	3.	31.	3.	12.	9.
122	17.	3.	34.	8.	7.	4.
123	11.	4.	49.	5.	13.	5.
124	10.	9.	27.	6.	10.	3.
125	15.	4.	25.	2.	9.	9.
126	13.	9.	36.	3.	9.	5.
127	8.	1.	27.	1.	13.	5.
128	10.	6.	28.	6.	7.	4.
129	9.	2.	34.	2.	10.	3.
130	12.	3.	31.	4.	6.	3.
131	7.	5.	30.	3.	7.	4.
132	11.	4.	27.	2.	3.	0.
133	11.	8.	28.	4.	8.	6.
134	8.	5.	32.	7.	6.	5.
135	2.	4.	26.	2.	5.	6.
136	4.	4.	20.	3.	3.	5.
137	6.	2.	23.	4.	4.	6.
138	6.	3.	17.	6.	3.	4.
139	10.	2.	15.	4.	6.	5.
140	2.	4.	15.	2.	2.	5.
141	9.	6.	16.	3.	8.	10.
142	4.	3.	10.	6.	6.	5.
143	5.	3.	11.	2.	4.	2.
144	10.	4.	15.	4.	0.	2.
145	5.	5.	15.	2.	1.	3.
146	4.	2.	14.	1.	3.	8.
147	4.	2.	8.	3.	2.	4.
148	1.	2.	11.	5.	7.	1.
149	4.	4.	12.	3.	5.	2.
150	6.	4.	9.	5.	2.	5.
151	3.	1.	16.	2.	1.	2.
152	9.	2.	20.	3.	1.	1.
153	0.	3.	10.	3.	4.	0.
154	3.	4.	12.	5.	2.	4.
155	2.	0.	21.	1.	1.	2.
156	4.	4.	8.	4.	2.	3.
157	5.	0.	11.	2.	4.	3.
158	2.	2.	7.	1.	2.	2.
159	4.	1.	11.	4.	2.	3.
160	3.	4.	7.	3.	3.	2.
161	4.	5.	7.	0.	0.	4.
162	4.	4.	12.	1.	2.	1.
163	2.	1.	13.	0.	0.	5.
164	3.	1.	5.	1.	2.	3.
165	0.	2.	12.	4.	2.	1.
166	2.	3.	4.	3.	0.	3.
167	2.	0.	8.	1.	2.	1.
168	1.	2.	10.	4.	3.	3.

5.3 MEASUREMENTS OVER THE PLOWED FIELD

As soon as measurements were completed at the dry-lake bed, the collimator was reloaded onto the truck and driven about 2 miles north to another part of the playa which had been plowed previously, as described in Section 4 (6-in. furrows every 30 in. over a square area 1500 ft on a side). The furrows ran north and south. The collimator was pointed west. The collection of data began at approximately H + 33 hr. Data were gathered from dusk until shortly after dawn. Barometric pressures varied from 26.60 to 26.66 in. of Hg.

Figure 4.6 shows the location and orientation of the collimator at the plowed field.

The local radiation survey at the plowed field was accomplished by having the scouting team drive around the plowed area in the carryall and taking readings with a survey meter.

Table 5.4 shows part of the actual data. Since counting rates were lower here than at the dry-lake bed site, live times of 20 min. were used.

5.4 MEASUREMENTS OVER ROUGH DESERT TERRAIN

On the evening of D + 5 day, the mobile laboratory was driven to a point 8 miles east of GZ. The area was typical desert terrain, as illustrated in Fig. 4.7. The collimator was pointed toward GZ. The ground sloped 2° downward from the chosen site toward GZ. A profile of the terrain is shown in Fig. 4.10.

A local radiation survey was obtained, as in the case of the dry-lake bed, by having a man with a survey meter walk from the collimator toward GZ. Results of the survey are shown by Table 5.5.

Table 5.6 shows part of the actual data. Live times of 8 min. were used.

In Tables 5.3, 5.4, and 5.6, the relative values of data and background counting rates can be observed.

The total number of counts in the worst case (plowed ground, looking toward the zenith) was approximately two and one-half times background. In the most favorable case (looking just below the horizon of the rough terrain) the total number of counts was approximately 50 times background. The other spectra ranged between these limits.

TABLE 5.4
COUNTING RATE PER ANALYZER CHANNEL AT PLOWED FIELD

CHANNEL NO.	ELEVATION 0		ELEVATION 85		ELEVATION 180	
	DATA	BKGD.	DATA	BKGD.*	DATA	BKGD.
1	305.	0.	2.	183.	3.	2.
2	1122.	24.	33.	1286.	46.	30.
3	316.	124.	286.	400.	198.	153.
4	379.	159.	494.	181.	342.	189.
5	391.	134.	589.	145.	454.	156.
6	389.	218.	642.	161.	633.	230.
7	508.	334.	887.	315.	855.	315.
8	551.	261.	863.	253.	871.	235.
9	635.	201.	978.	233.	804.	202.
10	572.	173.	947.	160.	708.	148.
11	581.	108.	956.	115.	608.	119.
12	577.	111.	967.	116.	514.	138.

TABLE 5.4 (Continued)
COUNTING RATE PER ANALYZER CHANNEL AT PLOWED FIELD

CHANNEL NO.	ELEVATION 0		ELEVATION 85		ELEVATION 180	
	DATA	BKGD.	DATA	BKGD.*	DATA	BKGD.
13	535.	127.	867.	113.	505.	144.
14	626.	126.	1087.	139.	474.	140.
15	700.	113.	1419.	149.	441.	129.
16	585.	143.	1137.	150.	402.	121.
17	450.	123.	752.	128.	382.	130.
18	436.	121.	725.	139.	344.	131.
19	417.	131.	688.	140.	351.	142.
20	449.	126.	709.	143.	319.	155.
21	408.	132.	670.	140.	339.	146.
22	448.	160.	726.	140.	340.	155.
23	456.	128.	846.	135.	273.	136.
24	462.	142.	851.	142.	285.	139.
25	357.	142.	731.	131.	230.	120.
26	309.	106.	602.	104.	192.	117.
27	297.	90.	567.	102.	179.	95.
28	286.	92.	560.	91.	179.	106.
29	315.	83.	664.	90.	152.	71.
30	302.	78.	652.	95.	131.	102.
31	273.	90.	661.	76.	125.	97.
32	243.	82.	566.	82.	139.	81.
33	250.	79.	506.	82.	120.	105.
34	242.	72.	454.	82.	110.	82.
35	210.	80.	428.	97.	99.	88.
36	198.	80.	478.	78.	96.	76.
37	168.	75.	402.	66.	81.	57.
38	184.	70.	416.	67.	100.	57.
39	141.	72.	335.	69.	71.	66.
40	138.	60.	327.	59.	99.	68.
41	140.	54.	344.	62.	82.	61.
42	133.	52.	324.	59.	70.	38.
43	136.	57.	352.	61.	74.	54.
44	127.	65.	341.	51.	90.	52.
45	142.	50.	338.	49.	79.	58.
46	104.	59.	325.	54.	76.	64.
47	111.	54.	364.	61.	81.	46.
48	150.	59.	373.	40.	68.	72.
49	187.	56.	389.	54.	77.	57.
50	210.	43.	477.	52.	68.	47.
51	214.	51.	513.	53.	89.	51.
52	190.	39.	613.	34.	70.	59.
53	157.	39.	561.	48.	78.	41.
54	164.	45.	547.	38.	64.	51.
55	133.	41.	384.	41.	57.	33.
56	125.	40.	350.	41.	64.	38.
57	116.	37.	280.	31.	75.	29.
58	103.	50.	245.	46.	46.	54.
59	110.	41.	212.	37.	48.	32.
60	130.	46.	261.	40.	61.	36.
61	147.	40.	310.	39.	68.	44.
62	170.	37.	398.	43.	55.	44.
63	192.	43.	551.	42.	74.	37.
64	214.	31.	640.	22.	66.	36.
65	234.	32.	701.	27.	50.	27.
66	185.	33.	629.	37.	71.	16.
67	134.	26.	580.	27.	59.	29.
68	140.	32.	440.	27.	44.	31.
69	125.	20.	50.	24.	44.	37.

TABLE 5.4 (Continued)
COUNTING RATE PER ANALYZER CHANNEL AT PLOWED FIELD

CHANNEL NO.	ELEVATION 0		ELEVATION 85		ELEVATION 180	
	DATA	BKGD.	DATA	BKGD.*	DATA	BKGD.
70	128.	31.	361.	31.	42.	19.
71	168.	18.	421.	27.	43.	31.
72	165.	38.	457.	25.	43.	32.
73	172.	37.	495.	27.	69.	26.
74	151.	29.	438.	32.	56.	28.
75	130.	42.	456.	28.	44.	30.
76	123.	20.	399.	33.	51.	24.
77	99.	27.	336.	30.	35.	28.
78	82.	27.	242.	17.	35.	20.
79	49.	30.	187.	30.	50.	27.
80	72.	24.	139.	30.	38.	21.
81	52.	24.	120.	18.	44.	24.
82	54.	20.	105.	24.	29.	25.
83	51.	20.	94.	13.	42.	22.
84	42.	23.	92.	25.	42.	21.
85	43.	12.	79.	17.	43.	24.
86	43.	24.	93.	14.	35.	19.
87	40.	14.	82.	23.	27.	18.
88	45.	21.	78.	19.	67.	17.
89	38.	19.	71.	22.	31.	18.
90	37.	18.	75.	21.	34.	17.
91	43.	16.	85.	20.	21.	9.
92	39.	13.	83.	21.	29.	15.
93	33.	16.	64.	17.	25.	18.
94	44.	16.	51.	17.	20.	15.
95	35.	15.	68.	11.	24.	19.
96	36.	10.	70.	18.	33.	16.
97	33.	9.	70.	8.	37.	12.
98	41.	7.	70.	24.	30.	13.
99	33.	20.	57.	18.	29.	14.
100	32.	13.	67.	13.	29.	11.
101	27.	11.	72.	8.	22.	9.
102	40.	13.	63.	15.	29.	16.
103	30.	14.	54.	14.	32.	18.
104	24.	13.	52.	20.	31.	10.
105	29.	13.	69.	14.	25.	13.
106	35.	13.	52.	17.	37.	19.
107	37.	12.	48.	18.	29.	11.
108	31.	21.	39.	15.	34.	11.
109	35.	15.	53.	15.	32.	10.
110	41.	11.	40.	6.	32.	14.
111	45.	11.	59.	16.	30.	14.
112	30.	13.	52.	20.	22.	17.
113	31.	12.	55.	13.	35.	18.
114	25.	12.	50.	15.	20.	14.
115	33.	15.	55.	15.	15.	12.
116	31.	6.	37.	9.	17.	17.
117	16.	8.	37.	9.	23.	9.
118	23.	10.	34.	13.	18.	11.
119	15.	20.	41.	12.	17.	9.
120	20.	8.	36.	11.	16.	11.
121	18.	12.	46.	11.	14.	5.
122	28.	12.	39.	6.	21.	15.
123	26.	5.	52.	9.	13.	13.
124	21.	4.	44.	16.	13.	9.
125	29.	11.	40.	7.	28.	6.
126	27.	12.	43.	9.	20.	14.

TABLE 5.4 (Continued)
COUNTING RATE PER ANALYZER CHANNEL AT PLOWED FIELD

CHANNEL NO.	ELEVATION 0		ELEVATION 85		ELEVATION 180	
	DATA	BKGD.	DATA	BKGD.*	DATA	BKGD.
127	29.	10.	46.	7.	25.	13.
128	26.	6.	40.	13.	22.	8.
129	30.	7.	39.	10.	28.	5.
130	19.	14.	32.	8.	8.	6.
131	19.	10.	31.	12.	23.	10.
132	19.	15.	46.	2.	16.	9.
133	19.	12.	26.	9.	15.	8.
134	15.	12.	45.	11.	11.	8.
135	16.	9.	25.	11.	7.	12.
136	18.	9.	31.	13.	9.	9.
137	13.	17.	34.	17.	17.	12.
138	17.	9.	19.	12.	11.	9.
139	11.	10.	21.	10.	10.	10.
140	11.	7.	16.	8.	13.	7.
141	17.	5.	24.	8.	15.	8.
142	10.	6.	18.	10.	10.	8.
143	5.	14.	15.	13.	11.	10.
144	17.	7.	10.	7.	7.	10.
145	10.	4.	22.	10.	7.	5.
146	5.	6.	22.	9.	9.	7.
147	9.	7.	17.	4.	9.	7.
148	8.	1.	13.	9.	6.	6.
149	11.	6.	21.	7.	2.	2.
150	8.	6.	12.	6.	6.	7.
151	15.	7.	18.	4.	5.	5.
152	6.	5.	21.	7.	9.	8.
153	9.	6.	20.	9.	5.	6.
154	11.	9.	20.	8.	3.	7.
155	7.	3.	33.	7.	5.	7.
156	12.	2.	17.	7.	4.	5.
157	8.	8.	20.	2.	5.	3.
158	6.	9.	12.	4.	6.	6.
159	6.	2.	14.	6.	5.	6.
160	6.	2.	12.	1.	2.	6.
161	5.	3.	15.	7.	1.	10.
162	8.	4.	10.	6.	4.	5.
163	2.	8.	11.	1.	5.	5.
164	7.	2.	5.	5.	9.	3.
165	4.	2.	10.	2.	6.	7.
166	6.	2.	4.	4.	7.	8.
167	6.	10.	5.	2.	3.	5.
168	1.	3.	6.	7.	3.	5.

*BACKGROUND SPECTRA WERE NOT MEASURED AT EVERY ELEVATION ANGLE. ACTUALLY THE 80° BACKGROUND WAS SUBTRACTED FROM THE 85° DATA. HERE NOTE AGAIN THE NOISE IN LOW CHANNELS.

TABLE 5.5
RADIATION SURVEY AT ROUGH TERRAIN

DISTANCE FROM COLLIMATOR, ft	DOSE RATE, mr/hr
100	18.5
200	19.5
300	18.5
400	19.0
500	19.0
600	19.5
700	19.0
800	19.5
900	19.0
1000	20.0

TABLE 5.6
COUNTING RATE PER ANALYZER CHANNEL AT ROUGH DESERT LOCATION

CHANNEL NO.	ELEVATION 0*		ELEVATION 80		ELEVATION 180	
	DATA	BKGD.	DATA	BKGD.	DATA	BKGD.
1	13.	2.	39.	2.	18.	2.
2	157.	24.	343.	18.	182.	25.
3	1027.	66.	1732.	71.	797.	86.
4	2137.	92.	3877.	78.	1653.	82.
5	1860.	79.	3639.	73.	2388.	91.
6	1496.	120.	3719.	125.	3631.	119.
7	2111.	165.	4557.	155.	4155.	126.
8	2773.	137.	5717.	119.	4320.	112.
9	3650.	122.	6932.	113.	4235.	110.
10	4248.	89.	7752.	84.	3877.	99.
11	4342.	94.	7368.	79.	3439.	72.
12	3769.	105.	6576.	70.	2509.	92.
13	3443.	116.	6602.	67.	1991.	81.
14	5262.	112.	11579.	81.	1877.	88.
15	7001.	95.	17397.	83.	1573.	84.
16	4018.	98.	9982.	72.	1413.	86.
17	2336.	98.	4439.	72.	1292.	89.
18	2186.	102.	3928.	71.	1172.	94.
19	1973.	94.	3953.	74.	1112.	84.
20	1819.	93.	3560.	77.	1062.	116.
21	1653.	101.	3281.	89.	935.	96.
22	1865.	107.	3611.	78.	844.	107.
23	2137.	106.	4651.	87.	701.	105.
24	1830.	104.	4335.	64.	689.	93.
25	1431.	87.	3268.	72.	513.	94.
26	1177.	74.	2479.	56.	442.	64.
27	1201.	66.	2456.	69.	378.	89.
28	1289.	72.	2852.	61.	364.	78.
29	1316.	82.	3442.	63.	304.	70.
30	1358.	63.	3716.	60.	255.	76.
31	1290.	58.	3375.	52.	217.	73.
32	1078.	60.	3113.	61.	172.	82.
33	965.	70.	2862.	49.	163.	66.
34	902.	72.	2836.	39.	130.	67.
35	912.	67.	2894	44.	122.	50.

TABLE 5.6 (Continued)
COUNTING RATE PER ANALYZER CHANNEL AT ROUGH DESERT LOCATION

CHANNEL NO.	ELEVATION 0*		ELEVATION 80		ELEVATION 180	
	DATA	BKGD.	DATA	BKGD.	DATA.	BKGD.
36	960.	67.	2902.	45.	103.	49.
37	848.	66.	2887.	53.	99.	56.
38	682.	64.	2469.	39.	74.	61.
39	598.	45.	1921.	40.	71.	51.
40	415.	64.	1583.	46.	83.	61.
41	450.	69.	1502.	31.	68.	51.
42	442.	62.	1541.	32.	70.	48.
43	420.	57.	1631.	38.	57.	51.
44	465.	39.	1715.	42.	66.	34.
45	446.	50.	1678.	42.	46.	43.
46	543.	58.	1955.	35.	60.	54.
47	713.	62.	2251.	37.	66.	57.
48	766.	55.	2680.	38.	50.	51.
49	827.	47.	3029.	41.	66.	43.
50	825.	52.	3082.	45.	63.	41.
51	753.	52.	2869.	42.	50.	48.
52	686.	40.	2551.	41.	61.	43.
53	574.	37.	2254.	28.	63.	35.
54	466.	42.	1990.	34.	48.	35.
55	410.	43.	1601.	27.	45.	35.
56	288.	30.	1285.	18.	44.	36.
57	256.	52.	1083.	21.	39.	36.
58	259.	33.	1011.	30.	42.	53.
59	269.	36.	1028.	20.	36.	41.
60	293.	36.	1045.	36.	46.	42.
61	324.	39.	1241.	25.	41.	44.
62	406.	55.	1366.	29.	59.	39.
63	481.	46.	1660.	29.	50.	45.
64	592.	43.	2013.	31.	43.	24.
65	670.	55.	2356.	22.	38.	31.
66	654.	32.	2545.	31.	47.	39.
67	587.	27.	2341.	14.	42.	28.
68	500.	35.	2100.	18.	39.	26.
69	493.	36.	1861.	23.	45.	33.
70	512.	40.	1812.	22.	36.	29.
71	560.	27.	1887.	17.	46.	31.
72	612.	43.	2161.	22.	39.	36.
73	635.	38.	2429.	38.	44.	28.
74	684.	35.	2559.	28.	35.	41.
75	659.	31.	2507.	21.	35.	20.
76	586.	31.	2381.	27.	32.	25.
77	473.	39.	2029.	25.	40.	31.
78	378.	29.	1752.	18.	36.	27.
79	305.	34.	1422.	24.	27.	23.
80	302.	27.	1201.	17.	34.	27.
81	247.	28.	927.	29.	33.	29.
82	188.	33.	787.	20.	30.	26.
83	194.	22.	617.	14.	26.	28.
84	156.	19.	552.	16.	34.	39.
85	134.	35.	471.	15.	29.	29.
86	112.	26.	483.	17.	30.	26.
87	130.	31.	407.	23.	33.	27.
88	127.	21.	374.	11.	34.	38.
89	134.	32.	410.	17.	34.	28.
90	136.	27.	429.	23.	31.	35.
91	150.	28.	439.	19.	27.	24.

TABLE 5.6 (Continued)
COUNTING RATE PER ANALYZER CHANNEL AT ROUGH DESERT LOCATION

CHANNEL NO.	ELEVATION 0*		ELEVATION 80		ELEVATION 180	
	DATA	BKGD.	DATA	BKGD.	DATA	BKGD.
92	135.	26.	452.	17.	27.	33.
93	124.	25.	417.	17.	30.	26.
94	101.	25.	432.	12.	23.	25.
95	119.	26.	367.	15.	37.	16.
96	85.	25.	367.	19.	26.	21.
97	83.	17.	272.	13.	27.	20.
98	83.	28.	305.	19.	27.	16.
99	85.	24.	271.	16.	29.	18.
100	66.	28.	251.	9.	23.	16.
101	74.	22.	246.	7.	37.	19.
102	79.	15.	247.	16.	24.	17.
103	80.	27.	225.	23.	21.	16.
104	68.	27.	244.	19.	30.	29.
105	80.	26.	282.	19.	27.	16.
106	92.	25.	245.	14.	21.	21.
107	73.	22.	271.	15.	19.	16.
108	73.	17.	251.	12.	29.	16.
109	72.	24.	238.	13.	23.	21.
110	81.	26.	254.	15.	27.	23.
111	78.	24.	258.	14.	22.	21.
112	74.	34.	243.	20.	18.	16.
113	74.	25.	264.	13.	26.	11.
114	73.	16.	223.	16.	24.	17.
115	67.	17.	252.	8.	23.	19.
116	66.	12.	207.	11.	24.	15.
117	50.	22.	210.	11.	18.	15.
118	51.	21.	200.	8.	25.	20.
119	55.	10.	197.	7.	26.	16.
120	61.	19.	215.	11.	18.	15.
121	48.	15.	202.	12.	17.	15.
122	66.	13.	221.	10.	23.	11.
123	46.	9.	218.	7.	8.	16.
124	58.	15.	211.	10.	16.	11.
125	67.	19.	207.	6.	23.	14.
126	63.	15.	240.	8.	25.	18.
127	68.	15.	208.	10.	24.	14.
128	74.	13.	219.	13.	15.	19.
129	66.	17.	214.	6.	19.	16.
130	50.	12.	194.	8.	15.	20.
131	66.	14.	194.	11.	17.	19.
132	41.	17.	197.	9.	14.	20.
133	50.	10.	175.	9.	12.	7.
134	49.	17.	182.	8.	19.	16.
135	59.	8.	160.	10.	13.	11.
136	43.	14.	189.	8.	14.	12.
137	38.	10.	139.	10.	18.	9.
138	39.	9.	154.	9.	14.	12.

TABLE 5.6 (Continued)
COUNTING RATE PER ANALYZER CHANNEL AT ROUGH DESERT LOCATION

CHANNEL NO.	ELEVATION 0*		ELEVATION 80		ELEVATION 180	
	DATA	BKGD.	DATA	BKGD.	DATA	BKGD.
139	42.	9.	139.	8.	17.	11.
140	37.	8.	129.	6.	18.	5.
141.	34.	9.	145.	7.	15.	8.
142	40.	22.	110.	7.	15.	13.
143	39.	13.	101.	6.	19.	12.
144	40.	17.	130.	5.	10.	16.
145	39.	12.	145.	7.	8.	10.
146	45.	13.	148.	5.	6.	8.
147	67.	12.	160.	5.	17.	7.
148	69.	10.	209.	10.	8.	6.
149	100.	18.	268.	12.	12.	9.
150	105.	17.	344.	4.	11.	12.
151	108.	14.	452.	4.	15.	8.
152	137.	17.	534.	5.	23.	16.
153	143.	6.	631.	7.	14.	17.
154	170.	9.	645.	7.	13.	9.
155	141.	4.	641.	7.	7.	14.
156	138.	12.	613.	7.	13.	6.
157	99.	14.	545.	4.	11.	7.
158	74.	4.	397.	1.	10.	6.
159	54.	6.	346.	5.	14.	16.
160	54.	7.	254.	3.	2.	7.
161	22.	2.	175.	2.	3.	5.
162	15.	3.	145.	8.	4.	2.
163	14.	4.	90.	7.	7.	8.
164	9.	7.	54.	2.	4.	2.
165	11.	6.	55.	1.	4.	3.
166	4.	5.	33.	3.	3.	2.
167	6.	3.	19.	3.	4.	2.
168	15.	3.	22.	3.	5.	4.

*ELEVATIONS ANGLES WITH RESPECT TO A PLUMB LINE ARE GIVEN HERE.

A CORRECTION FOR THE 2° NEGATIVE SLOPE OF THE GROUND WAS MADE IN THE DATA ANALYSIS.

Chapter 6

ANALYSIS OF RESULTS

6.1 INTERPRETATION OF DOSE-VERSUS-HEIGHT MEASUREMENTS

In Fig. 5.1 the dose rate is plotted as a function of height above the third experimental site, typical desert terrain. The theoretical curve which gave the best fit to the data was the calculated curve of Spencer[1] for an equivalent distance ρ of 40 ft of air corresponding to the ground-roughness effects. The theoretical curve for dose-vs-height above a smooth infinite plane is shown in Fig. 2.2. The result of ρ = 40 ft will be compared with the results and interpretation of the angular distribution of dose, to be discussed in later sections of this chapter.

Other investigators have found various values for ρ. Mather[2] found ρ = 15 ft for a type of terrain very similar to, but perhaps not as rough as, the rough terrain reported here, although he used a different technique for determining ρ. He did not make dose-vs-height measurements. Other experimental measurements comparable to those reported here were performed by Schuert[3] and by Shumway[4].

Predictions were made in the O.C.D. Engineering Manual[5] that ρ would be from 10 to 20 ft over a graveled area and from 20 to 60 ft above a plowed field. Spencer[1] suggested that ρ = 40 ft may be a reasonable value for a natural Nevada field.

The measured directional sensitivity to Co^{60} gamma radiation of the detector used for the dose-vs-height measurements is shown in Fig. 6.1. The ion chamber was enclosed in a box of 1/4-in. plywood with approximately 1 in. of polyurethane foam directly surrounding the detector. The box was suspended so that the cable connector was at the top. The detector-box combination had a slightly lower sensitivity at the window end than at the sides. There was also a more noticeable decrease in sensitivity at the connector end. However, consideration of the angular distribution of dose (Fig. 2.1) over a fallout plane shows that the detector was oriented so that the dose contribution was least from the directions for which the anisotropy was greatest. The error in measured dose due to detector anisotropy should therefore be negligible.

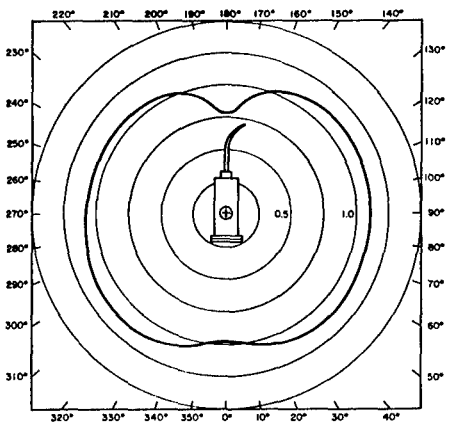

Fig. 6.1 – Relative directional response of nuclear Chicago cutie pie ionization chamber used in field. Response relative to Co^{60}.

6.2 ANALYSIS OF SPECTRA

6.2.1 *Background Correction.* During the course of the experiment backgrounds were taken after each spectrum, except in the case of the plowed ground where, because of time limitations, the same background was used for two different angles in a few cases where the angles were close together. In no case was the background taken at a time greater than 20 min from the time of the data run, so that it was not considered necessary to adjust the background for decay. The measured background spectra did not represent the true background due to the fact that the calibration sources were closer to the crystal of the spectrometer when the collimator was open than when the collimator was closed. Counts taken in a low-radiation environment showed the presence of a definite Cs^{137} and Co^{60} background spectrum, with a slightly higher count rate for the open position than for the closed position of the aperture wheel. This effect was noticed before the experiment but time did not permit modification of the collimator to eliminate it. To correct for this spectrum, a 100-min count was taken with the aperture wheel in the collimator-open position, but with the aperture plugged with a solid lead insert. A 100-min background count with the aperture wheel in the collimator-closed position was subtracted from this, leaving, presumably, only the net $Co^{60} - Cs^{137}$ difference in background spectrum. Appropriate percentages of this difference spectrum were added to the various backgrounds according to their respective live times.

6.2.2 *Gainshift Corrections.* Because of extreme environmental conditions and shortage of preparation time, it was not possible to obtain and maintain the precise zero-energy level and gain calibrations which would be required in laboratory analysis for isotope concentration. Temperature control in the collimator was sacrificed because the greater internal volume required in the shield would have resulted either in less shielding (and higher backgrounds) or an unacceptably greater weight of shield.

In the course of the experiment, wide temperature variations were encountered, producing correspondingly rapid changes in the gain of the detector. Frequent calibration spectra were run, and the amplifier gain was adjusted correspondingly. An effort was made to keep the Cs^{137} 661-kev peak near channel 66 for a nominal gain of approximately 10 kev per channel. In most cases, the location of this peak changed less than 2 channels between calibrations.

In the analysis of the data the gain calibration for a given spectrum was obtained by assuming that the time rate of change of gain was constant between calibrations, permitting the use of a linear interpolation to obtain the average channel location of the Cs^{137} peak. Based upon the position of the Cs^{137} photopeak, an appropriate computer program was used to convert the gain to 10 kev per channel for each spectrum measurement.

6.2.3 *Gamma-Ray Spectrum Unfolding Program.* Various methods are available for unfolding gamma-ray spectra that can be broadly classified as iterative unfolding and stripping methods.

Inasmuch as our primary interest was in the dose, we chose the iterative method of Scofield[6] as being sufficiently accurate for our purposes and perhaps less sensitive to small errors in zero-energy level and gain calibration. Response of the collimator-detector combination to gamma rays of various energies was determined by using several monoenergetic point sources in 4π mounts. These sources were moved at uniform speed through a rectangular pattern to simulate an area source. From the spectra obtain with these monoenergetic sources, a response matrix was generated. This response matrix was used with Scofield's iterative unfolding program, slightly modified to adapt it to the capabilities of our computer facility. The experimental calibration of the collimated detector and the computer programs used are discussed in Appendix B.

6.2.4 *Decay Corrections.* The gamma-ray spectrum of fallout radiationchanges continuously with time, with peaks of various energies appearing and disappearing as primary fission products

decay and daughter products accumulate. Rather than try to generate some method of handling these individual spectrum changes, it was more relevant to our problem simply to consider the change in total dose rate, which can be handled conveniently by the well known $t^{-1.2}$ law. It was therefore assumed that there were no gross changes in spectral distribution during the period between the beginning and the end of measurements at a given location (less than 12 hr).

6.3 GAMMA-RAY SPECTRA

The method used to obtain gamma-ray energy spectra from pulse-height distributions will be described in Appendix B. The data from each group of four consecutive channels were lumped to produce energy spectra with 40-kev intervals.

After the channels were grouped, some channels showed a negative number of counts, due to normal statistical fluctuations in the background count level. A negative count is meaningless to the unfolding program so these counts were set to zero. Since positive as well as negative fluctuations in the background count rate were expected, this would have resulted in a slight positive bias for channels where the count rate was zero or nearly zero. Therefore, a "zero criterion" was used such that if the net count in a given channel was not greater than the square root of the sum of the data count plus the background count, the count of that channel was set to zero.

A few counts with energies up to 2.5 Mev appeared in the raw data, especially at the rough terrain. However, the counting rates at these high energies were too low to allow a quantitative analysis.

6.3.1 *Gamma-Ray Spectra Over Dry-Lake Bed.* Figures 6.2 and 6.3 present the unfolded gamma-ray spectra at various angles over the dry-lake bed. (By convention, the orientation is considered to be 0° when the collimator is looking straight down at the ground.) Points are plotted at the center of each 40-kev interval.

It is interesting to note that the low-energy peak appears at about 140-kev for angles below the horizon and at about 100 kev for angles above the horizon.

Figure 6.4 shows the energy content per energy interval at an elevation of 85°. The height of each box of the histogram represents the energy content within the box. To permit direct intercomparison, the energy intervals were chosen to be the same as those chosen by Spencer[1] and by Clarke[7]. The agreement is satisfactory.

6.3.2 *Gamma-Ray Spectra Over Plowed Field.* Figures 6.5 and 6.6 present the unfolded gamma-ray spectra at various angles over the plowed field. Note that the spectra are almost identical to those above the dry-lake bed. Measurements at this field were taken at about H + 30 hrs for angles below the horizon.

6.3.3 *Gamma-Ray Spectra Above Rough Desert Terrain.* Figures 6.7 and 6.8 present the unfolded gamma-ray spectra at various angles above the rough desert terrain. These data were taken at about D + 5-1/2 days. Compared with spectra from the other two locations, spectra taken at angles below the horizon showed substantial increase in high-energy radiation. The peak at channel 38 was assumed to be the 1.6-Mev peak from La^{140}. Its displacement from channel 40 was assumed to be caused by slight nonlinearity of the detector. In spite of the increased number of high-energy photons in the direct radiation, the spectra of the scattered radiation from angles above the horizon were about the same as those above the other terrains, indicating that the energy and angular distribution of skyshine radiation is relatively independent of ground roughness and of spectrum changes in the direct radiation.

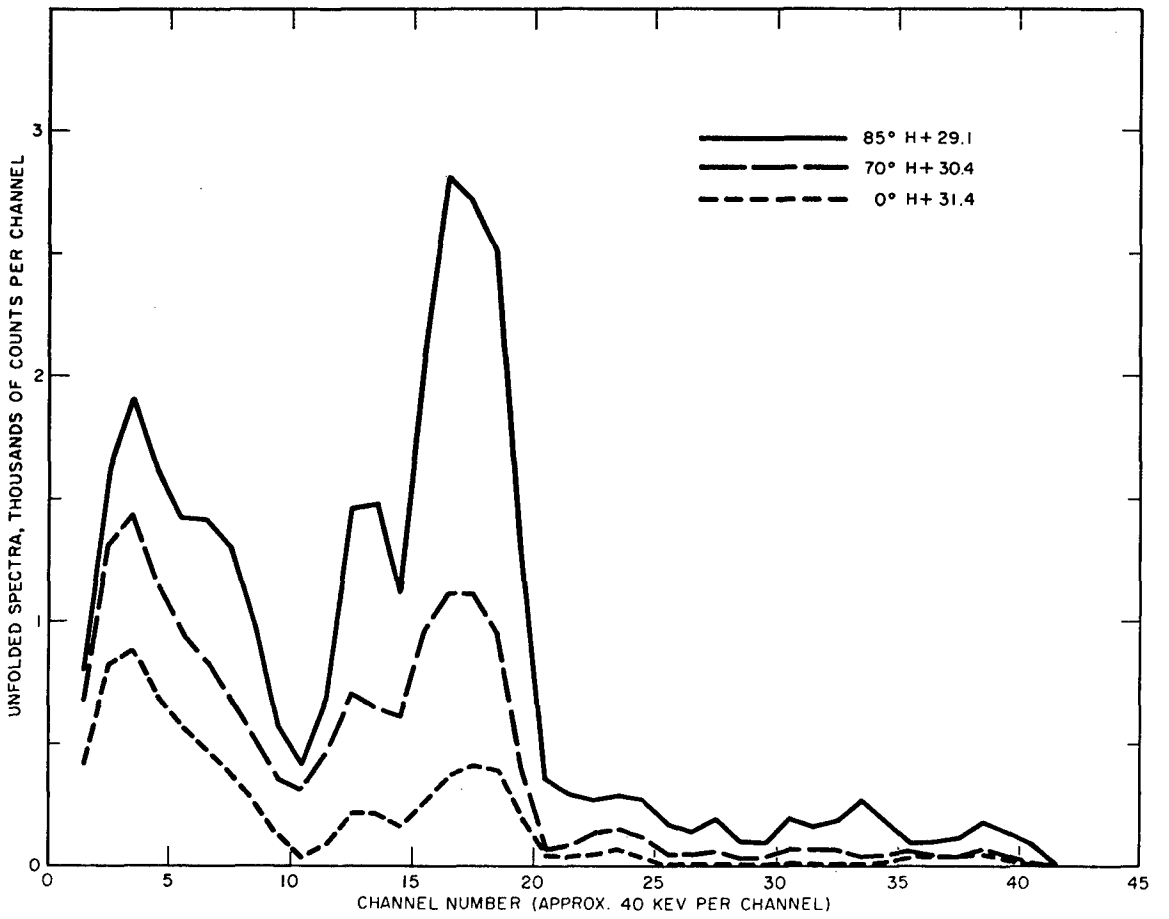

Fig. 6.2 – Unfolded gamma-ray spectra at dry-lake bed.

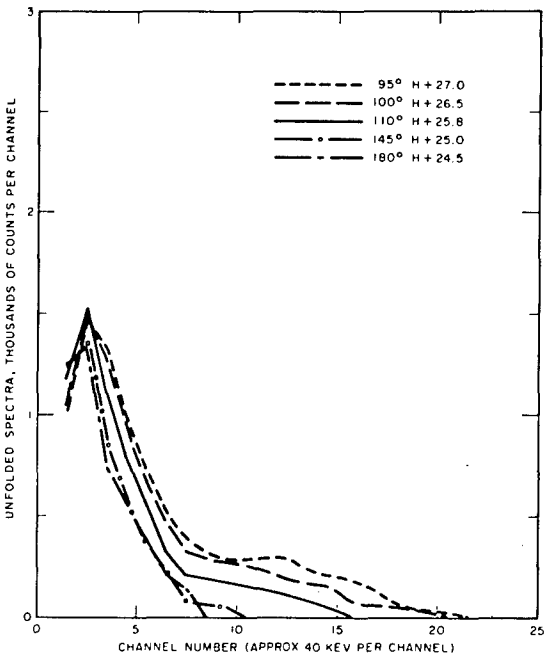

Fig. 6.3 – Unfolded gamma-ray spectra at dry-lake bed.

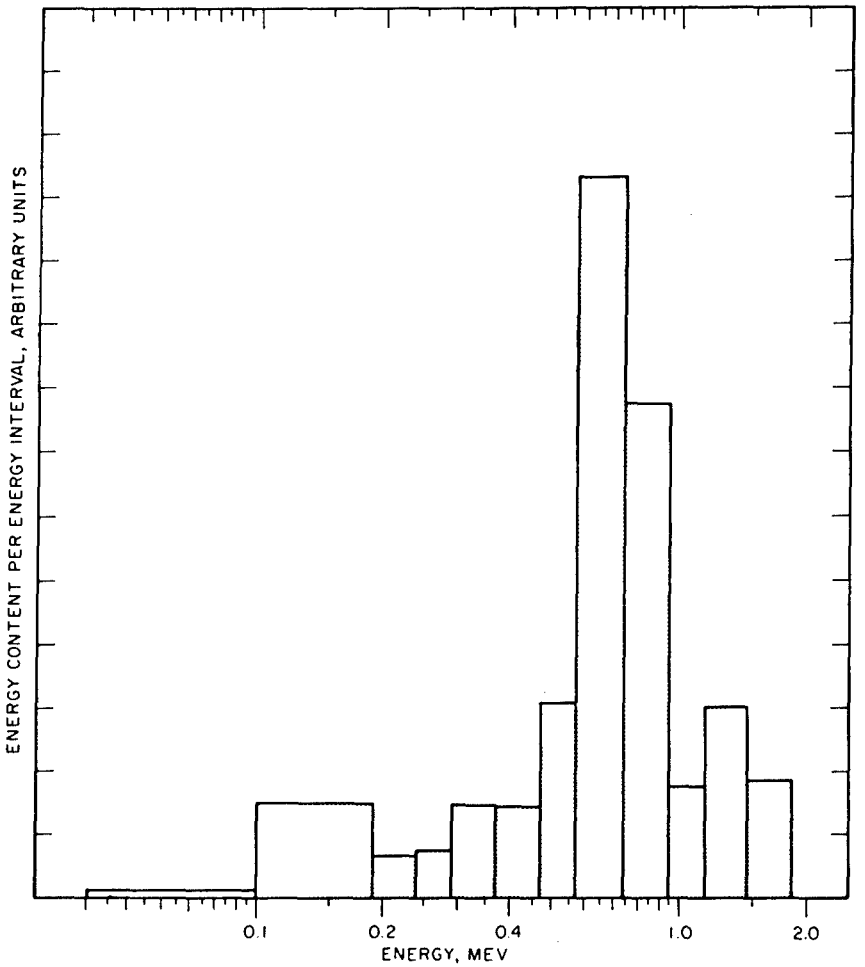

Fig. 6.4 – Energy content per energy interval at 85° at dry-lake bed (H + 29.1).

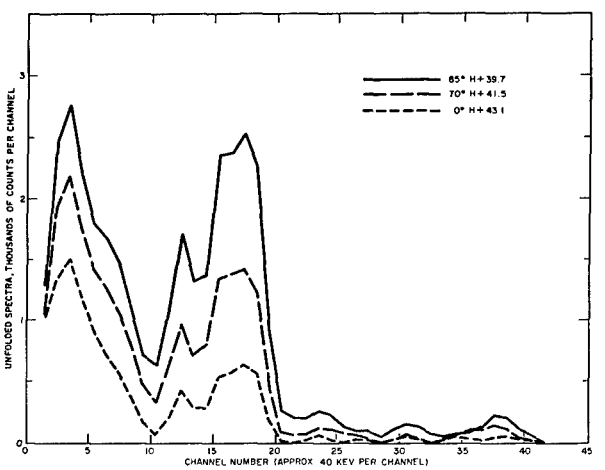

Fig. 6.5 – Unfolded gamma-ray spectra at plowed field.

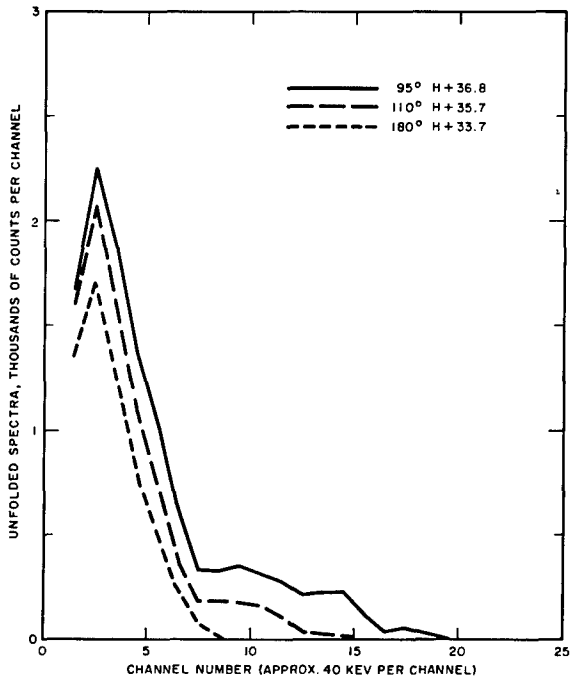

Fig. 6.6 – Unfolded gamma-ray spectra at plowed field.

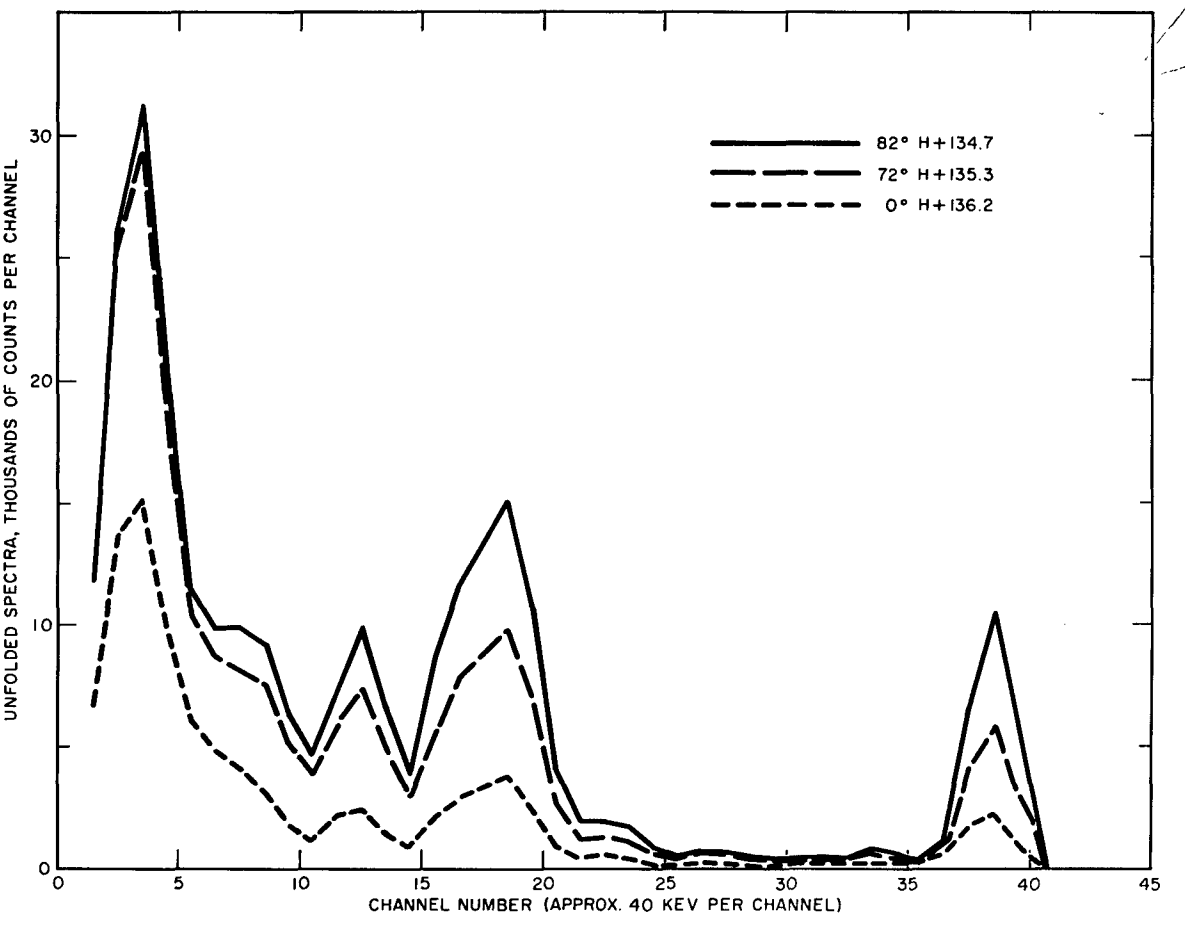

Fig. 6.7 – Unfolded gamma-ray spectra at rough desert terrain.

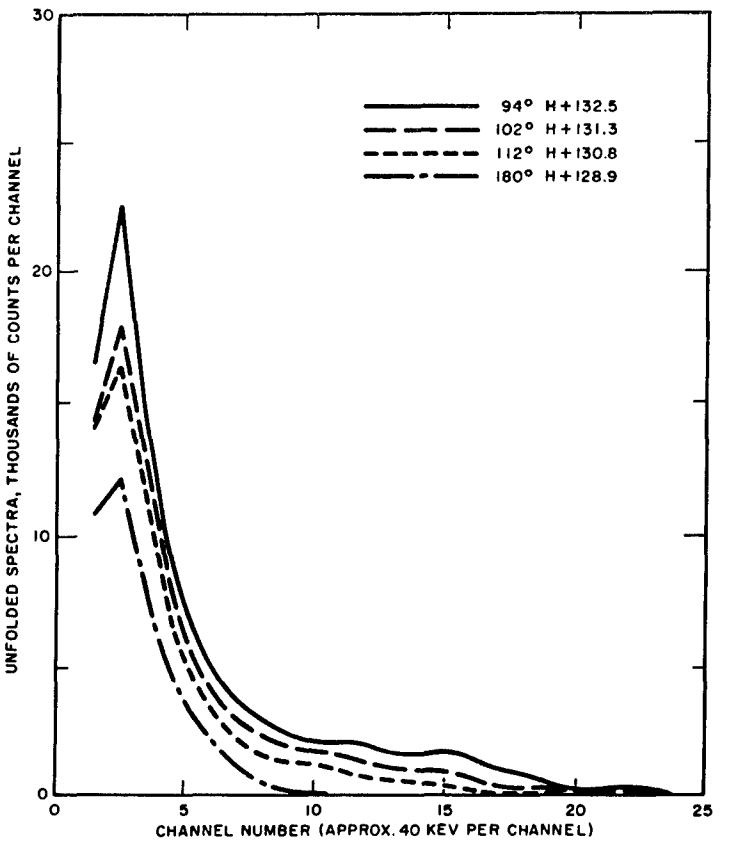

Fig. 6.8 – Unfolded gamma-ray spectra at rough desert terrain.

Figure 6.9 presents the energy content per energy interval at an elevation of 82°. The peak at about 1.6 Mev is quite prominent.

6.3.4 *Comparison.* Table 6.1 presents some comparative values from the spectral data. The values in the table are unfolded counts per channel normalized to the 0° data for the particular terrain and energy interval concerned. The photon flux increases with angle within a given energy interval. However, the increase is more rapid with higher energies, indicating a hardening of the spectra as one approaches the horizon. Within the energy interval 640 to 680 kev there is a greater increase with angle over the dry-lake bed than over the plowed field, presumably caused by a shielding effect of the roughness of the plowed field.

6.4 DOSE-ANGULAR DISTRIBUTIONS

6.4.1 *Angular Distribution of Dose over Dry-Lake Bed.* Figure 6.10 shows the angular distribution of dose 3 ft above the dry-lake-bed position. After gamma-ray spectra were unfolded using the method described in Appendix B, dose was calculated for each angle from the appropriate gamma-ray energy spectrum.

The dose was calculated by multiplying together the unfolded gamma-ray energy spectrum and a curve[8] for dose-per-unit energy versus energy. More particularly a curve was plotted showing the relationship between energy and dose-per-unit energy, according to Goldstein[8]. The value of the curve was read for the midpoint energy of each of the 40-kev-wide channels; this value (at the midpoint) was multiplied by the number of counts in the channel and by the midpoint energy of the channel. The summation of these point-by-point triple products is proportional to dose.

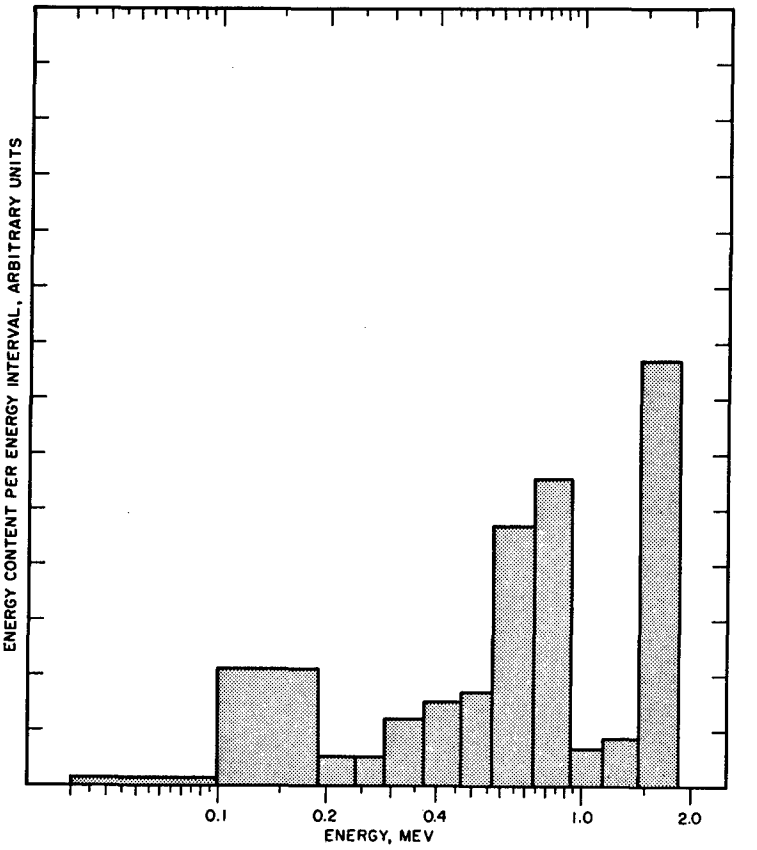

Fig. 6.9 – Energy content per energy interval at 82° at rough desert terrain (H + 134.7).

TABLE 6.1
UNFOLDED COUNTS PER CHANNEL NORMALIZED TO DATA AT 0° ELEVATION

CHANNEL, KEV	0°	35°	70°	72°	80°	82°	85°
DRY-LAKE BED							
120–160	1.0	1.36	1.63		1.98		2.16
640–680	1.0	1.61	3.16		5.09		7.94
1520–1560	1.0	1.31	1.80		7.53		9.72
PLOWED FIELD							
120–160	1.0	1.17	1.45		1.51		1.84
640–680	1.0	1.30	2.42		2.93		4.17
1520–1560	1.0	0.90	2.12		2.27		3.63
ROUGH TERRAIN							
120–160	1.0	1.10		1.93		2.06	
720–680	1.0	1.13		2.69		4.13	
1520–1560	1.0	1.00		2.71		4.85	

The dose (actually a quantity proportional to dose, since the constant correction factor for the collimator solid angle was not applied) was then decay-corrected according to $t^{-1.2}$, where t is time after detonation. The time chosen for decay correction was the mean time at which the spectrum was measured.

Examination of Figure. 6.10 shows that good agreement is found between the experimental results and the theoretical curve [9] for an equivalent height of 20 ft. Agreement between experimental and theoretical values could be improved in the region of the abrupt increase at the horizon by considering the angular resolution of the collimator. Experimental values at other elevation angles where the rate of change of dose rate with angle is less rapid are only slightly affected by angular resolution. The estimated ground-roughness air-equivalent distance at the dry-lake bed is 20 ft.

6.4.2 *Angular Distribution of Dose over Plowed Field.* Results of dose-angular-distribution measurements 3 ft above the plowed field are displayed in Fig. 6.11. Spencer's theoretical curves for air-equivalent distances of 40 and 60 ft are shown for comparison. The rate of change of dose with angle is much more rapid than would be expected for an equivalent height of 40 ft, although the maximum intensity is about what would be expected for this height. An explanation for this will be discussed in Sec. 6–4.4.

6.4.3 *Angular Distribution of Dose over Rough Desert Terrain.* Results of measurements of angular distribution of dose at the typical rough desert site are shown in Fig. 6.12. The figure shows good agreement between experimental and theoretical values for an air-equivalent distance of 40 ft. This agrees with the air-equivalent distance (40 ft) based on dose-vs-height measurements at the same site.

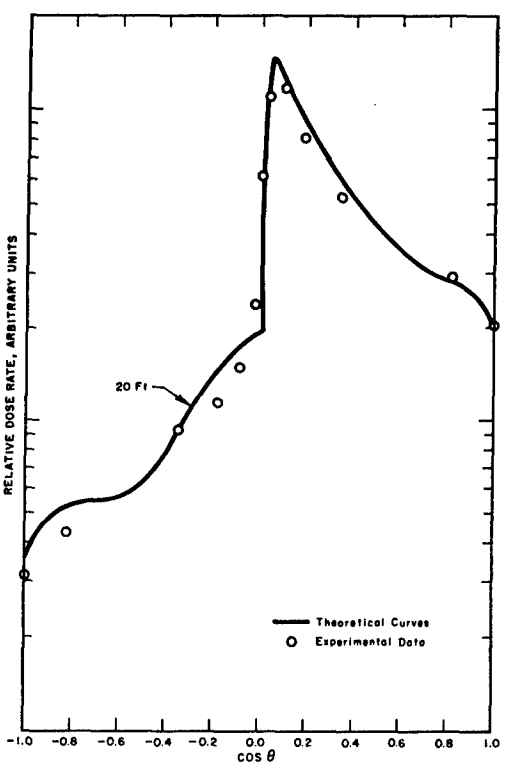

Fig. 6.10
Angular distribution of dose above dry-lake bed.

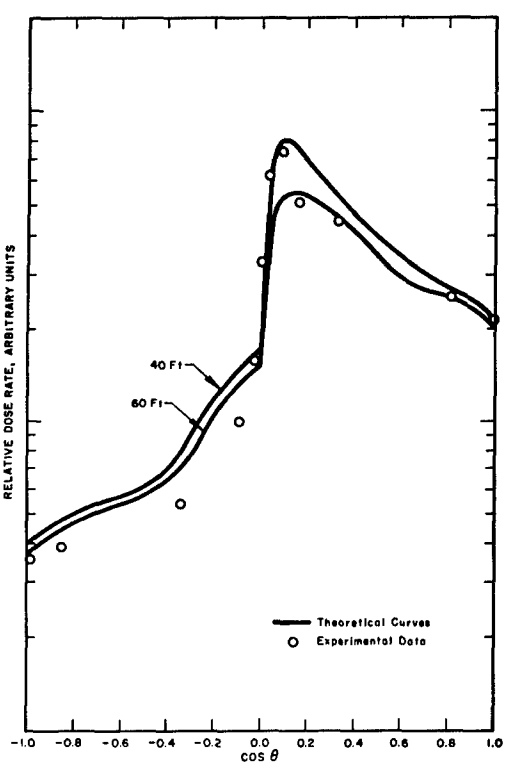

Fig. 6.11
Angular distribution of dose above plowed field.

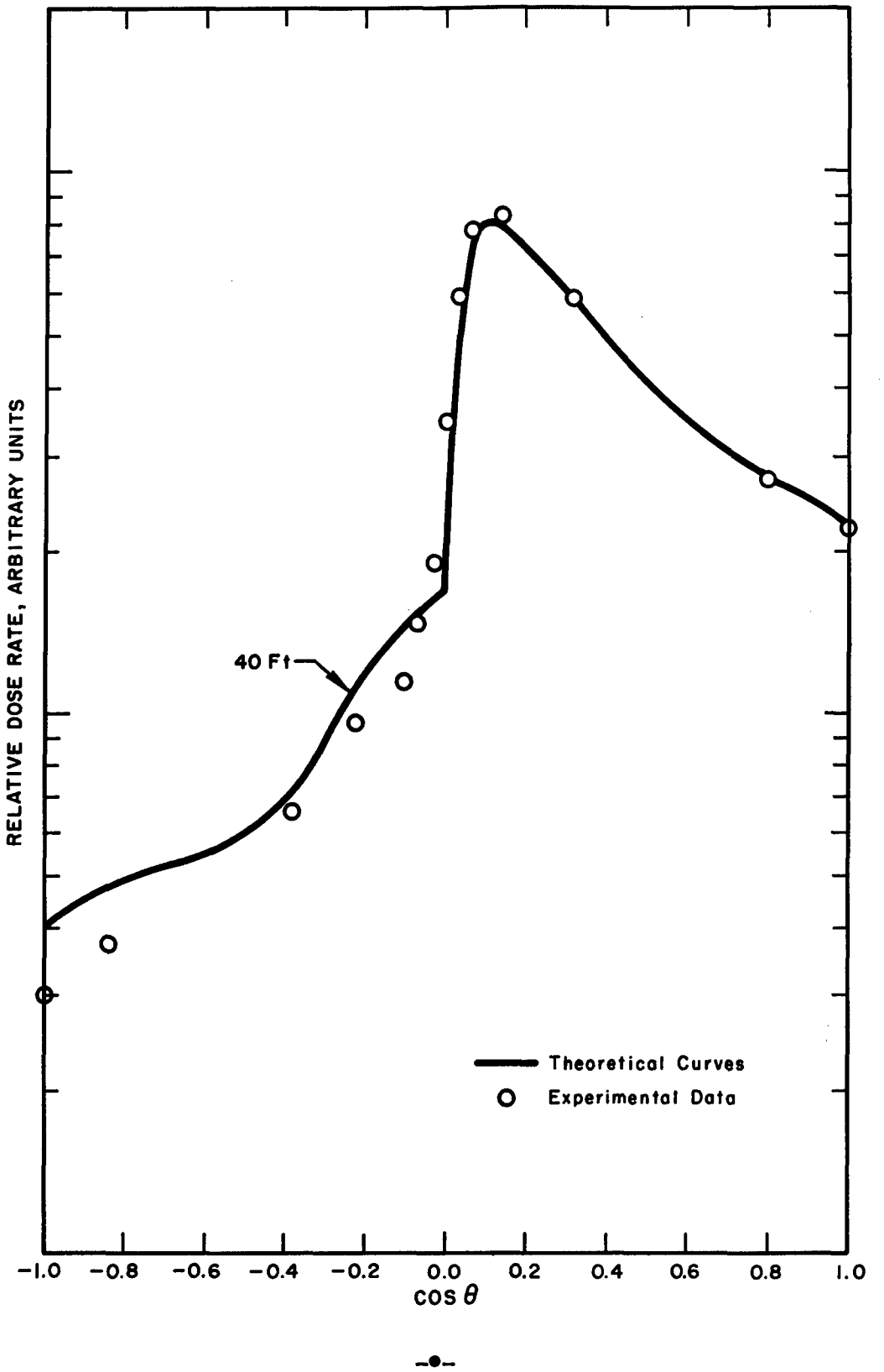

Fig. 6.12 – Angular distribution of dose above rough desert terrain.

6.4.4 *Comparisons Between the Different Sites.* It may be useful to make some observations from comparisons between the different dose-angular distributions measured at the three sites. The dry-lake bed was perhaps as smooth as any terrain likely to be found in nature. The surface consisted of water-deposited clay, baked dry and hard. These bare, smooth areas 1/2 to 1-1/2 miles wide, extended for several miles along the bottom of a broad valley. Except for the peculiar cracking pattern caused by the shrinking of the clay as it dried (see Figs. 4.1 and 4.2), the surface was very flat for several thousand feet from the collimator. Still, the measured dose-angular distribution indicated that the slight surface irregularities gave significant shielding at the collimator elevation.

On the other hand, the rough desert terrain was probably much more broken in surface detail and in overall structure than the majority of terrains which would be encountered in fallout calculations. The ground surface consisted of coarse gravel, giving a rough, porous surface. One might expect a *priori* that there would be a great difference in air-equivalent distance between the flat lake bed and the rough desert terrain. The difference was at most a factor of two, however, and the difference in effective shielding was slight. For those two sites, the approximate theoretical treatment of ground roughness which assumes an air-equivalent distance agrees with the experimental results.

As was noted before, however, the measured dose-angular distribution over the plowed ground did not correlate well with any of the theoretical curves. Referring again to Fig. 6.11, note that the data points near the horizon where the count rate was highest, and the data therefore most reliable, show the greatest discrepancy from the theoretical curve. Since the locations of the measurements over the plowed field and the dry-lake bed were near each other, and the time after the event was about the same for both measurements, it is reasonable to expect that some comparisons might be possible.

Consider the profile of the plowed field, Fig. 4.6; at angles less than about 45°, the detector saw the entire source directly. At angles greater than 45°, progressively more of the source in the furrows was hidden by the shoulders of the rows until, at the horizon, all of the source in the furrows was effectively buried beneath the surface of the ground, and made, therefore, a negligible direct contribution to dose at the detector. At the horizon the effective source strength for direct radiation was reduced to about 0.6 of what it would have been for smooth ground.

To make an approximate calculation of the shielding effect of the rows, the following assumptions were made:

1. Source concentrations were proportional to the dose calculated from the zero-degree spectrum (the detector looking directly at the ground).

2. For the angles for which there was significant shielding of direct radiation, the distance from source to detector was great enough that the distance from one side of a furrow to the other was negligible, and that the photons were parallel incident at the detector.

3. Buildup in the ground was negligible.

4. At low angles above the horizon the major contribution to dose was due to single or multiple scattering of photons at small angles. This small-angle scattering was eliminated for the portion of the source in the furrows.

Using these assumptions, we calculated a relative source strength, S_p/S_f, i.e., the relative strength of the source seen by the collimator over the plowed ground compared to a source of the same concentration on the dry-lake bed. We assumed that the concentration was equal on all surfaces. As was noted before, for angles less than 45°, the source was seen directly without shielding, so that $S_p/S_f = 1$ for angles less than 45°. For angles between 45° and 90°, the source was partially hidden by the furrows. Referring to Fig, 6.13, the portion of the source seen

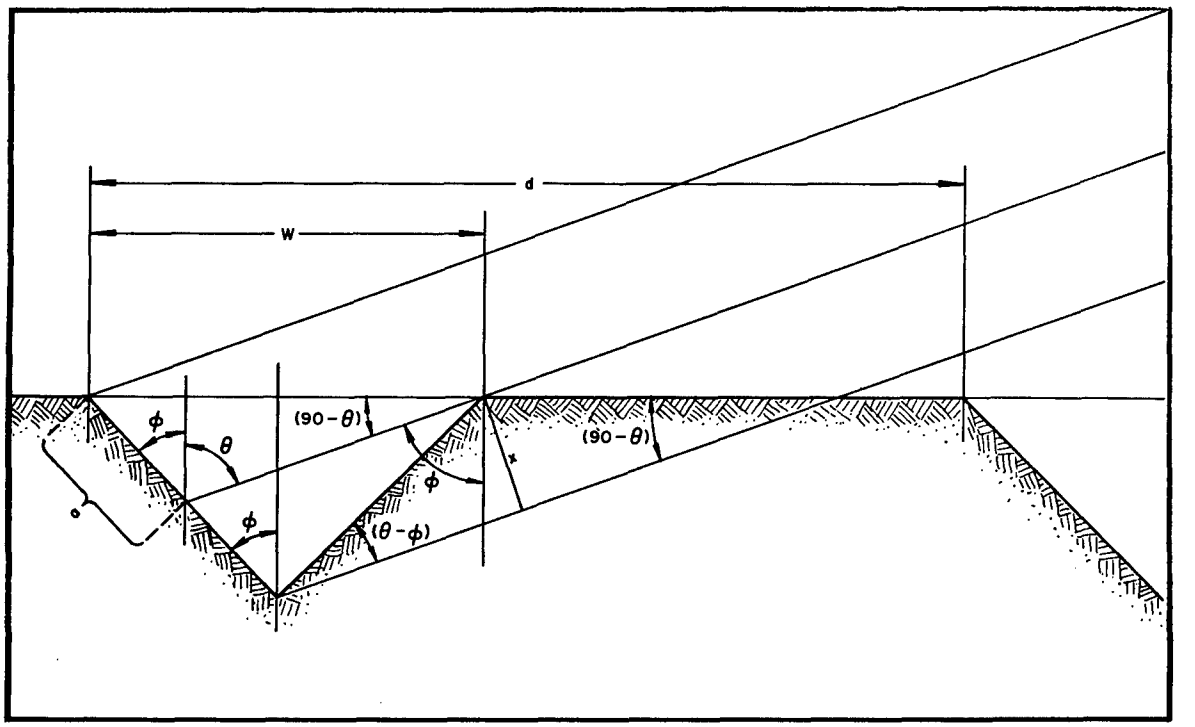

Fig. 6.13 – Profile of plowed ground.

by the collimator at angle θ was:

$$S_p = k \left[(d-w) + a + F(x) \right]$$

where k = concentration per unit area

d = distance between furrows

w = width of furrows

a = portion of furrow seen directly

F(x) = function which gives contribution from hidden parts of furrow

From the law of sines

$$\frac{a}{\sin (90-\theta)} = \frac{w}{\sin (\theta + \phi)}$$

$$a = \frac{w \sin (90-\theta)}{\sin (\theta+\phi)}$$

To calculate F(x), let dF be an element of the beam of photons that arrives at the detector from the activity in the shielded part of the furrow. Then,

$$dF = \left[\frac{dx}{\cos (\phi + \theta 90)} + \frac{dx}{\cos (\theta + 90 - \theta} \right] e^{-\mu t(x)}$$

where x is the perpendicular distance across the beam and t(x) is the thickness of earth traversed by a given element of the beam. Obtaining t(x).

$$t(x) = x \cot (\theta - \phi) + x \cot (90 - \theta)$$

Integrating across the beam, starting from the element that is grazing incident at the edge of the row (x = 0) and ending with the element that originates at the bottom of the furrow

$$F(x) = k\left[\frac{1}{\cos(\phi+\theta-90)} + \frac{1}{\cos(\phi+90-\theta)}\right]\int_0^{\left[\text{x max}\right]} e^{\mu\left[\cot(\theta-\phi)+\cot(90-\theta)\right]x}\,dx$$

$$F(x) = \frac{-k}{\mu}\left[\frac{1}{\cos(\phi+\theta-90)} + \frac{1}{\cos(\phi+90-\theta)}\right]\left[\frac{1}{\cot(\theta-\phi)+\cot(90-\theta)}\right]$$

$$\left[1-e^{-\mu(\cot(\theta-\phi)+\cot(90-\theta))\left(\frac{w\sin(\theta-\phi)}{2\sin\phi}\right)}\right]$$

where x max = $\left[\ w \sin(\theta-\phi)\ \right] / (2\sin\phi)$

Using the above equations for α and F(x), S_p/S_f was calculated for each of the angles between 45° and 90° at which measurements were made. For the present case, d = 30 in., w = 12 in., μ = 0.23 in., and ϕ = 45°.

For angles from 90° to 110°, the effective source was assumed to be solely that portion of the source on the surface of the rows between the furrows (cf Assumption 4). This neglects the contribution due to large angle scattering of photons from the source in the furrows. However, since the probability of large-angle scattering was small, and the energy of photons scattered at large angles was greatly reduced, this assumption should introduce only a slight error. For these angles, S_p/S_f = 0.6.

For angles near the zenith, all radiation reaching the detector must be scattered at large angles and the effective shielding due to the rows would be negligible. For these angles, S_p/S_f = 1.0.

To compare data from the plowed field and the dry-lake bed, we assume that for both cases the decay-corrected dose at 0° was proportional to the source strength. Using the calculated dose at various angles, the relative source strengths, and the values for S_p/S_f at various angles, we calculated what the dose from the dry-lake-bed source would be if it were partly shielded in a manner similar to the plowed-field source. The normalized results are listed in Table 6.2 with the measured dose from the plowed ground shown for comparison. The two sets of values are plotted for comparison in Fig. 6.14.

TABLE 6.2
COMPARISON OF CALCULATED AND MEASURED VALUES FOR PLOWED GROUND

θ, DEGREES	S_p/S_f	$D_f(S_p/S_f)$	D_p
0	1.0	0.22	0.22
35	1.0	0.31	0.28
70	0.84	0.46	0.46
80	0.75	0.63	0.53
85	0.65	0.81	0.76
88	0.62	0.71	0.65
90	0.60	0.38	0.34
92	0.60	0.15	0.16
95	0.60	0.094	0.10
110	0.60	0.056	0.054
135	1.0	0.045	0.040
180	1.0	0.032	0.036

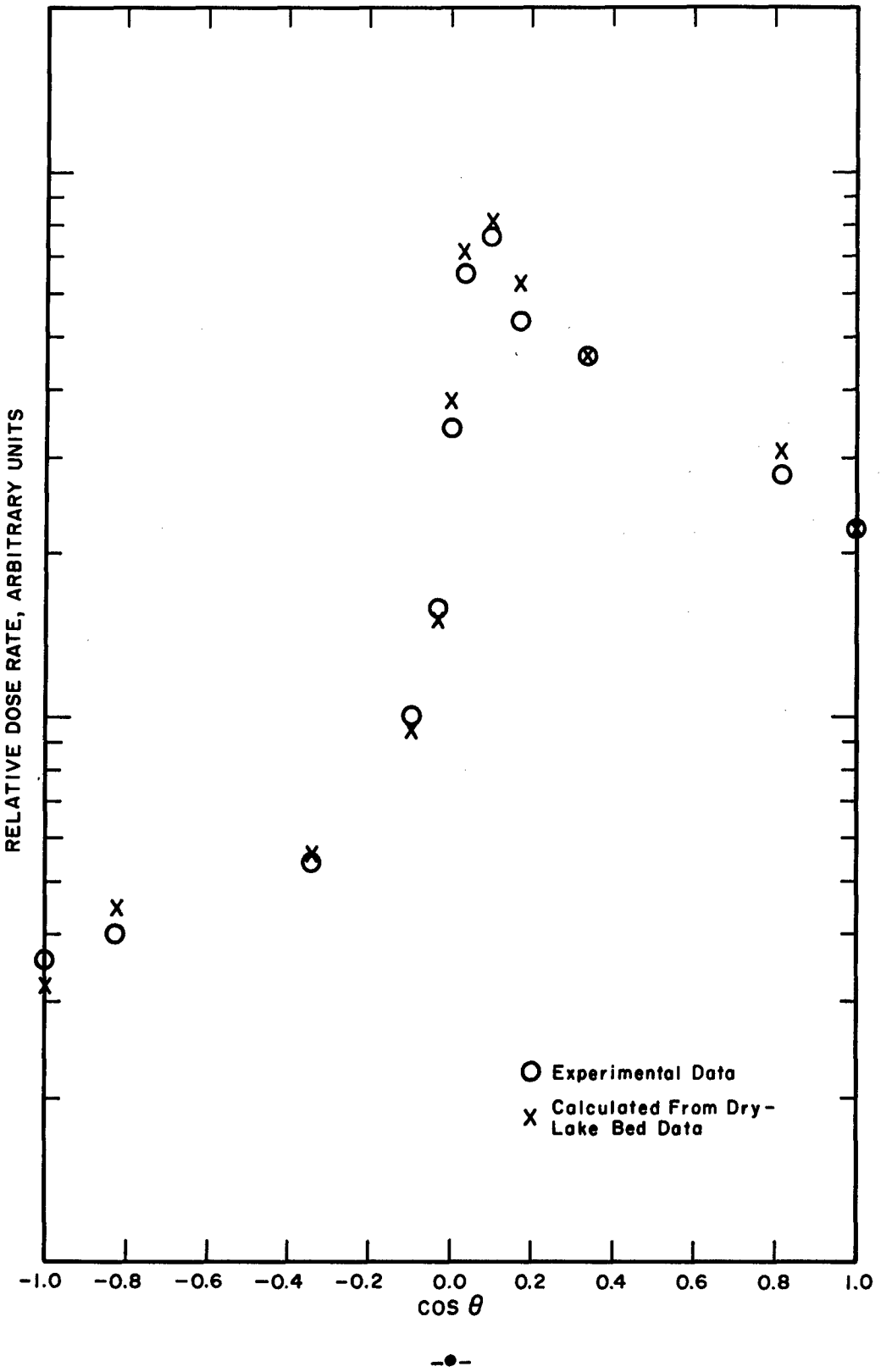

Fig. 6.14 – Comparison of dry-lake bed and plowed-field data.

The fine surface structure of the plowed ground was, of course, much more broken after plowing than that of the dry-lake bed. This broken surface decreased intensities from angles near 90°, as the comparison indicates.

6.5 DOSE-RATE MEASUREMENTS AT 3 FT

The dose rate at 3 ft above ground was measured by using 0-10 mr, 0-200 mr (Victoreen Model 239 and 362) and Victoreen condenserionization chambers. Several measurements were made with diverse instruments at each location. The average was taken as the dose rate at that point and was estimated to be accurate to within 5% of the true value.

Referring to Fig. 2.2 (Variation of Dose with Height) we obtained reduction factors associated with the air-equivalent distances determined from the dose-angular-distribution data. For the air-equivalent distance of 20 ft at the dry-lake bed, the reduction factor was 0.67, and for the rough desert terrain (40 ft) the reduction factor was 0.54.

Because of the anomalous shape of the dose-angular-distribution curve, and because this curve is valid only for azimuths perpendicular to the furrows, an air-equivalent distance was not obtained for the plowed field. However, for two different areas, the ratio of the reduction factors should be equal to the ratio of the measured dose rates normalized for source strength and corrected for decay. By comparing the measured dose rates and using the reduction factors obtained for the other two sites, we obtained a reduction factor for the plowed field. Comparison of plowed-field data with the dry-lake bed data gave a reduction factor of 0.55, and comparison of plowed-field data with the rough desert-terrain data gave a factor of 0.60. The average reduction factor for the plowed field, then, was 0.58. For plowed ground of sawtooth profile, Clifford[10] obtained an experimental reduction factor of 0.45, using Cs^{137}.

The collimated detector, pointed directly at the ground, should constitute a fairly good instrument for measuring fallout concentration. Accordingly ,a calculation was made of the dose rates expected from fallout of concentrations indicated by the gamma-ray spectra for 0° elevation. As a simple expedient, rather than calculating the dose-rate contribution of each of the various energies of the measured spectra, we calculated the concentration of Co^{60} or Cs^{137} which would have been required to produce an equivalent energy flux in the collimator. The dose rate for this concentration of Co^{60} or Cs^{137} on a smooth infinite plane was then multiplied by the appropriate reduction factor. The value obtained in this manner was taken to be the dose rate from the measured fallout concentration on the terrain being considered. Similar values were obtained using either isotope.

The measured dose rates for the dry-lake bed and the rough desert terrain were about 70% of the dose rates calculated from the spectrometer data. For the plowed ground, no independent calculation from the spectrometer data could be made, since the measured dose rate was used in obtaining the dose-reduction factor.

The ion chambers were essentially 4π detectors. The response of these detectors must equal the integral of the dose-angular distribution over all angles. The discrepancy between calculated and measured dose rates must, therefore, be due to an error in the calculated source strength. This is to be expected, inasmuch as no consideration was given to backscattering from the ground surface. Chilton[11] calculated that for a point source of Co^{60}, backscattering would introduce a 10% increase in dose, and for a point source of Cs^{137} the increase would be 15%. Although we are concerned here with an area source, these figures indicate the order of magnitude of the error involved. There may be an additional error which originates in the value for the strength of the sources used in calibrating the collimated detector. These source strengths were calculated from spectrometer measurements. Measurements with ion chambers indicated source strengths about 10% less than those obtained from the spectrometer measurements.

It is our opinion that the measured dose and the dose calculated from spectrometer measurements agree within the limits of error involved.

REFERENCES

1. L. V. Spencer, *Structure Shielding Against Fallout Radiation from Nuclear Weapons,* NBS Monograph 42, 1962.

2. R. L. Mather, R. F. Johnson, F. M. Tomnovec, and C. S. Cook, *Gamma Radiation Field Above Fallout Contaminated Ground,* Operation Teapot Report, WT-1225, May 1955.

3. WT-1465, E. A. Schuert, Project 32.4, *Fallout Studies and Assessment of Radiological Phenomena,* 1959 (Secret)

4. B. W. Shumway and S. Tomoeda, *Shielding Effectiveness of Compartmented Structures in a Fallout Field* (Unclassified – Official Use Only), Preliminary Report on Small Boy Project 2.14 (1962).

5. *Engineering Manual: Design and Review of Structures for Protection from Fallout Gamma Radiation,* Office of Civil Defense, Revised 1 October 1961.

6. N. E. Scofield, U. S. Naval Radiological Defense Laboratory Research and Development Technical Report USNRDL-TR-447, *A Technique for Unfolding Gamme-Ray Scintillation Spectrometer Pulse-Height Distribution,* 1960.

7. E. T. Clarke and J. O. Buchanan, *Radiation Shielding Against Fallout* Nucleonics, Vol, 20, No. 8, August 1962.

8. Herbert Goldstein, *The Attenuation of Gamma Rays and Neutrons in Reactor Shields,* Table 2.1, prepared by Nuclear Development Corp. for the U. S. AEC, 1957.

9. L. V. Spencer, Private Communication to C. M. Huddleston.

10. C. E. Clifford, *Effects of Ground Roughness on the Gamma Dose from Cs^{137} Contamination,* Defense Research Chemical Laboratories Report No. 401, Ottawa, March 1963.

11. A. B. Chilton, University of Illinois, *"Backscattering by an Infinite Concrete Plane of Gamma Radiation from a Point Isotropic Source,"* Trans, A.N.S., Vol. 6, #1, p. 200.

Chapter 7

CONCLUSION

It has been found that the shielding effectiveness against fallout radiation of three types of Nevada terrain can be accounted for on the basis of a model that treats the fallout as being uniformly buried beneath the surface of the earth. In the case of a dry-lake bed and in the case of typical desert terrain, values were found for air-equivalent distances of the effective hypothetical burial depth. The values found were 20 and 40 ft, respectively, for those two cases. Reasonable agreement was found with the results of other investigators, and there was fair consistency between the two results for air-equivalent distance obtained from the present experiment in the typical rough desert terrain where both dose-angular distribution and dose-versus-height measurements were made.

In the case of the radiation dose above a plowed field, the model had to be modified to take into account periodic variations in the ground level. The modified theory gave good agreement with experiment.

It was found that even a dry-lake bed, which is exceptionally smooth for a natural surface, does not correspond to a theoretically infinite and smooth plane. Dose-angular-distribution measurements indicated a dose-reduction factor of 0 .67 for the dry-lake bed. Similar measurements for rough desert terrain gave a reduction factor of 0.54. Ion-chamber measurements of dose versus height indicated a similar value. Comparison of ion-chamber measurements at the three locations, normalized for source strength and corrected for decay, indicated a dose-reduction factor of 0.58 for the plowed field. This compares with a reduction factor of 0.45 for plowed ground of a different (sawtooth) profile, obtained by Clifford[1], using Cs^{137} sources.

REFERENCES

1. C. E. Clifford, *Effects of Ground Roughness on the Gamma Dose from Cs^{137} Contamination*, Defense Research Chemical Laboratories Report No. 401, Ottawa, March 1963.

Appendix A

FALLOUT CONTOURS

For the experimenters to be prepared in advance, some predictions* had to be made concerning probable dose rates to be expected from fallout. The best operating characteristics of the equipment occurred in the 10– to 100–mr/hr range. Therefore, it was desirable to know probable locations of such radiation fields and to explore likely regions.

Fallout patterns can be described in terms of (1) infinity dose, (2) 1-hr reference dose-rate, or (3) dose-rate at time t after detonation.

Infinity dose at a given position means the total dose accumulated by an observer at the given position from 1 min after detonation until the fallout radiation has decayed to zero. The numerical value of the infinity dose, computed from 1 min after detonation, equals 11.3 times the 1-hr reference dose rate. The infinity dose is expressed in roentgens.

The 1-hr reference dose rate at a given position is the actual dose rate measured at that position in roentgens per hour, decay-corrected to H + 1. It should be noted that 1-hr reference dose rates are used even in connection with distances greater than the distance travelled in 1 hr by the assumed 15-mph wind. Actually, fallout at distances discussed here is not complete until several hours after detonation. The 1-hr reference dose rate is, however, a useful fiction. In all cases the dose and dose rate under discussion are at an elevation of 3 ft above the ground.

The dose rate D_t at time t hours after detonation is related to the 1-hr reference dose rate by

$$D = D_1 t^{-1.2} \qquad \text{(A.1)}$$

From Eq. A.1 and the proportionality between D_∞ and the 1-hr reference dose rate,

$$D_t = \frac{D_\infty}{11.3} t^{-1.2} \qquad \text{(A.2)}$$

At a time 24 hr after detonation,

$$t^{-1.2} = 24^{-1.2} = 0.0218$$

Therefore, the dose rate 24 hr after detonation is

$$D_{24} = \frac{D_\infty}{11.3} (0.0218) = 0.00193 D_\infty$$

---

* *The Effects of Nuclear Weapons*, 1957 edition, was used as a guide for predicting fallout patterns.

Table A.1 shows approximate residual radiation 1-hr reference dose rate contours on the ground for a 1-kt burst when the wind velocity is 15 mph.

The displacement of the center of the GZ circle is the distance downwind from the actual to the effective GZ position for drawing concentric circles of radiation contours. Downwind and crosswind distances are the major and minor axes of an elipse whose perimeter touches actual GZ and whose major axis is oriented downwind from GZ.

TABLE A.1
RESIDUAL–RADIATION CONTOURS

DOSE RATE, r/hr	RADIUS OF GZ CIRCLE, miles	DISPLACEMENT OF CENTER OF GZ CIRCLE, miles	DOWNWIND DISTANCE, miles	CROSSWIND DISTANCE, miles
1100	0.0368	0.0294	0.368	0.110
368	0.0828	0.0515	0.845	0.257
110	0.1510	0.0828	1.95	0.442
36.8	0.2425	0.1030	4.23	0.662
11	0.349	0.1323	8.28	0.1030
3.68	0.515	0.1543	18.39	0.1875

An approximate scaling law for surface bursts is

$$R = R_0 W^{1/3} \text{ at a distance } d = d_0 W^{1/3} \qquad (A.3)$$

where W is the fission yield of the weapon and R_0 is the 1-hr reference dose rate at a distance d_0 from GZ. This scaling law applies to any fallout-pattern contour.

From the scaling law of Eq. A.3 and the data in Table A.1, dose-rate contours can be determined for other yields. For example, the downwind distance from a 1-kt surface burst was computed for a radiation field of 100 mr/hr 24 hr after detonation when the wind velocity was 15 mph. For a 2-kt weapon, the distance for this dose rate increased to approximately 25 miles.

Doubling the downwind distance would reduce the downwind dose rate by a factor of approximately 3. Thus, for the 1-kt burst mentioned in the preceding paragraph, a downwind distance of 30 miles would reduce the downwind dose rate to about 30 mr/hr after 24 hr. For 2 kt, the corresponding distance would be 50 miles.

If the wind velocity is other than 15 mph, the distance from GZ for a given radiation contour in the downwind direction equals approximately the downwind distance for a 15-mph wind multiplied by the ratio of 15 to the actual wind velocity in miles per hour. It must be realized, however, that this approximation is very crude except for distances greater than 100 miles downwind.

Thus, areas out to several miles in the expected downwind direction had to be explored in advance so that the experimenters would be familiar with the territory.

Appendix B

RESPONSE MATRIX GENERATION AND SPECTRUM UNFOLDING

BY
D. BARNHILL and W. PAGE

The purpose of the Response Matrix Generation program is to generate a matrix which describes a particular response, according to our detector arrangement, of an NaI(Tl) scintillation detector. This response matrix corrects a measured gamma-ray spectrum to yield approximately the spectrum of photons actually incident at the entrance aperture of the collimator.

As there were only a few monoenergetic gamma-ray sources available for calibrating a detector, a means had to be found to synthesize monoenergetic spectra over the energy range desired. The problem, therefore, was to write a program which would synthesize gamma-ray spectra for specific energies, a criterion being that it would adequately reproduce the calibration spectra.

Nine gamma-ray sources were used to calibrate the collimated scintillation detector. An effort was made to obtain monoenergetic sources where possible, but some compromises were necessary in favor of sources with longer half-lives. The isotopes used were Cd^{109}, Hg^{203}, Cr^{51}, Be^{7}, Cs^{137}, Nb^{95}, Mn^{54}, Zn^{112}, and Y^{88}. In the case of Y^{88}, there are two gammas: one of 1.85 Mev and one of 0.9 Mev. A gain-shifted Mn^{54} spectrum (0.835 Mev) was subtracted from the Y^{88} spectrum to obtain the approximate distribution for the 1.85-Mev gamma spectrum.

Each calibration spectrum consists of a pulse-height distribution which may be represented by a histogram. Each bar on the histogram represents the number of counts in a particular channel. We consider each spectrum as being composed of the following components: a Compton plateau, a dip, and a Gaussian photopeak. Empirical equations represent each of these components as a function of the channel number for a given peak energy; that is, they are functions of both the photopeak energy and the channel. Each component was worked on separately and these regions were separated by specific points.

A semi-logarithmic display of the spectrum of the cesium area source is shown in Fig. B.1. Note that, because the detector is collimated, the Compton plateau is essentially a straight line with no backscatter peak. The valley is approximately parabolic in shape and covers the the spectrum from the Compton edge to the point on the photopeak that is equal in height to an extension of the Compton edge. The photopeak is a symmetrical Gaussian peak of the form $y = A_1 \exp(-(X-A_2)^2/A_3)$, where A_1 is the height of the photopeak, A_2 is the midpoint of the photopeak, and A_3 is related to width at a half-maximum of the photopeak. Straight lines were fitted to the Compton plateaus of each of the calibration spectra. Values were obtained for intercepts and slopes of these straight lines. A modified LSF 20 program was then used to fit polynomials to these parameters as a function of peak channel number. A similar approach was used to obtain polynomials for VXN, the abscissa of the vertex of the dip, and HIT, the maximum height of the photopeak. A function sub-program was incorporated to yield a linearly interpolated value of VYN, the ordinate of the vertex of the dip, as a function of the peak channel number. This linear interpolation was used as the calibration data's fluctuations precluded using polynomial

fits to the data unless several different polynomials were used, and the resultant values would not have necessarily been more accurate.

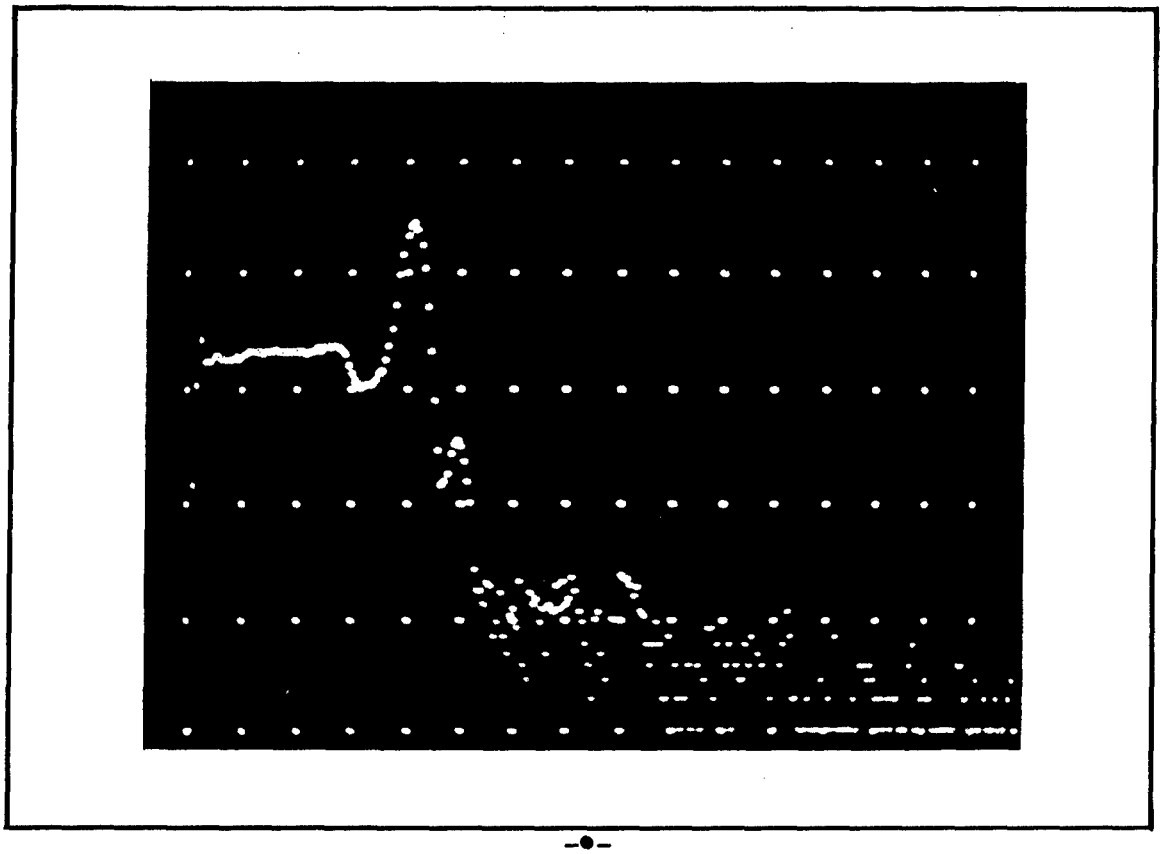

B.1 – Calibrated spectrum from simulated area source.

Table B.1 presents the program used to generate response matrix. The program first computed the parameters used for the spectrum (associated with a given peak energy) being synthesized and then, by successive testing to determine in which component of the spectrum each channel was located, it calculated the height, in counts, of each channel using the appropriate function. Each spectrum, or column of the matrix, was then summed and normalized. These normalized numbers were summed in groups of four so that they corresponded to the channel width used in unfolding.

While working on the program and testing different approaches and parameters, sense switches were used to provide options whereby unnormalized pulse heights could be punched out and data cards could be read in to have the program synthesize spectra for any desired peak energy. These options were left in the program listed here.

A diagram of a spectrum and a list of a few of the names and terms used are presented in Fig. B.2.

After the measured spectrum was subjected to corrections for background and gain shift, the data were grouped into 42 pulse-height channels each 40 kev wide. The spectrum could then be viewed as a 42-element column matrix C(n). In principle the C(i) can be transformed

into the matrix XK(i) by multiplying with the inverse of the response matrix (R(i j), i.e.,

$$XK(i) = R^{-1}(ij)C(i)$$

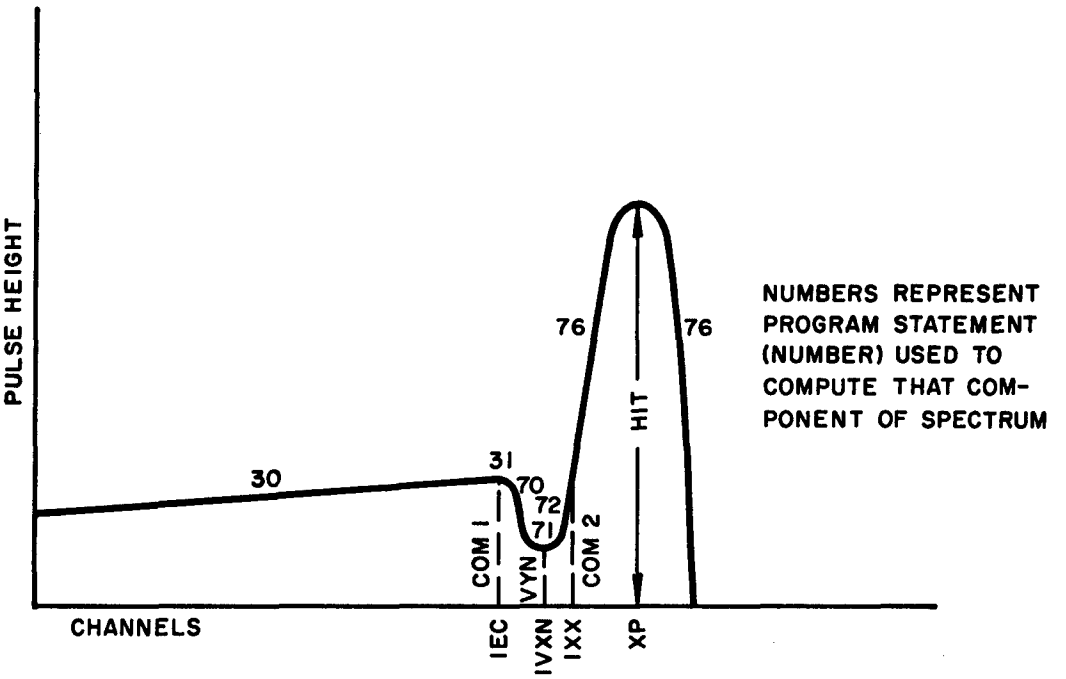

XP	PEAK ENERGY OF SPECTRA
X	CHANNEL NUMBER – RUNNING VARIABLE
VYN	ORDINATE OF VERTEX OF DIP
VXN	ABSCISSA OF VERTEX OF DIP
COM^1	COMPTON EDGE – FIRST POINT OF DIP
IEC	CHANNEL NUMBER OF COM^1
IVXN	CHANNEL OF VXN (truncated)
COM^2	ORDINATE OF FIRST POINT OF PHOTOPEAK (equal to COM^1)
IXX	CHANNEL NUMBER OF COM^2
HIT	MAXIMUM HEIGHT OF PEAK
P^1	PARAMETER USED IN COMPUTING LEFT SIDE OF DIP
P^2	PARAMETER USED IN COMPUTING RIGHT SIDE OF DIP

Fig. B.2. – Response of a collimated NaI(Tl) detector to a nonenergetic gamma-ray spectrum.

The problems inherent in inverting R to obtain R^{-1} exactly are well-known and generally defeat the applications of this direct calculation. An iterative technique for unfolding scintillation spectra has been developed by Scofield[1] and used successfully[1,2] for continuous spectra. Since our measured spectra have relatively simple structure and since we are interested in total dose rather than spectral analysis, it is felt that the limit of accuracy of our results is determined to a large extent by the actual spectral measurements and particularly by the detector calibration and response-matrix generation. Errors involved in the iterative unfolding scheme should be relatively minor.

Since the iterative unfolding scheme is described elsewhere, we shall describe it only briefly to fix the notations used in our Fortran code. Rather than finding the inverse response matrix $R^{-1}(ij)$ directly, we seek a diagonal matrix $D(ij)$ that will unfold the data directly so that:

$$XK(i) = D(ij)C(j)$$

A typical step in the iteration procedure would be:

$$XK = D \cdot C$$

$$XN = R \cdot XK$$

$$D'_{ii} = \frac{XKi}{XNi}$$

where D is an approximation to the final diagonal matrix, XK is an approximation to the final unfolded matrix, XN is an approximation to the measured matrix C, and D is the improved diagonal matrix formed from ratios of the elements of XK and XN. Using the unit matrix as a first approximation for D, the above iteration was carried out fifty times. Convergence of the result was checked by finding $\Sigma[XK_i - C_i]^2$ after each iteration. In case of divergence, the program terminates automatically and prints the result as well as the number of iterations for which the program became divergent. The program as listed (Table B.1) has provisions for smoothing either the input or output data; this feature was not used, however.

Table B.2 presents the program for spectrum unfolding and energy flux calculation.

TABLE B.1
RESPONSE MATRIX GENERATION

```
      DIMENSION SHAP(170), ASHAP(42)
4     FORMAT(15)
5     FORMAT(5E15.7)
      COMMON GNC
      GNC=1.0
      If (sense switch2) 6,7
6     READ 4, IP
      GO TO 8
7     DO 60 IP=10,168, 4
8     SHAP(169)= 0.0
      SHAP(170)= 0.0
C     CALCULATE CONSTANTS FOR EACH COLUMN.
      EP= 10*IP
      XP= IP
      XP=XP + .5
      WID = .63*XP**.5
C     THIS USES FUNCTION SUBPROGRAM TO GIVE ORDINATE OF VERTEX OF DIP.
      VYN = VYNF(XP)
```

TABLE B.1 – (Continued)
RESPONSE MATRIX GENERATION

```
C       CALCULATES ABSCISSA FOR VERTEX OF DIP.
        VXN = (((3.08645E-07*XP-1.1.0543E-04)*XP + 1.37306E-02)*XP+2.68745E-01)
        1*XP+1.97277E-00
        IVXN=VXN+.5
        VXN = IVXN
        HIT = ((((6.26266E-09*XP-2.99180E-06)*XP
        +5.17164E-04)*XP-3.66243E-02)*XP+5.71441E-01)*XP+3.59042E+01
        HIT = 1000.*HIT
        SUM = 0.0
        IF (IP-48) 10, 11, 11
10      A=6.10.-.419*XP
        GO TO 15
11      IF (IP-82) 12, 13, 13
12      A=800. - .69*(XP-65.)*(XP-65.)
        GO TO 15
13      A=610. - .419*XP
15      IF(EP-660.)16, 17, 17
16      B = ((1.75263E-10*EP-2.43096E-07)*EP+8.76461E-05)*EP+7.92890E-05
        GO TO 20
17      IF(EP-810.) 18, 19, 19
18      B = (((-3.48624E-13*EP + 2.25021E-11)*EP+1.11892E-06)*EP-1.11190E-03)
        1*EP+3.08553E-01
        GO TO 20
19      B=((-3.47637E-12*EP+1.66151E-08)*EP-2.80467E-05)*EP-1.76326E-02
20      EC=XP*(.18*LOGF(XP)-.05+.5
        IEC = EC
        EC = IEC
        COM1 = A*EXPF(B*EC*2.3)
        COM2=COM1
        XXX1 = XP+WID*SQRTF(.361*LOGF(HIT/COM1))
        XXX2 = XP-WID*SQRTF(.361*LOGF(HIT/COM1))
        IF(XXX1-XXX2) 21, 22, 22
21      XX=XXX1+.5
        GO TO 23
22      XX=XXX2+.5
23      IXX = XX
        XX = IXX
        P1 = ((EC-VXN)*(EC-VXN))/(4.*(COM1-VYN))
        P2 = ((XX-VXN)*(XX-VXN))/(4.*(COM2-VYN))
C       CALCULATE COUNTS PER CHANNEL
        Do 50 I= 1, 168
```

TABLE B.1 – (Continued)
RESPONSE MATRIX GENERATION

```
      X = I
      IF(I-IEC)30, 31, 32
C     COMPTON DISTRIBUTION
30    SHAP(I) = A*EXPF(B*X*2.3)
      GO TO 40
C     FIRST POINT OF COMPTON EDGE
31    SHAP(I) = COM1
      GO TO 40
32    IF(I-IVXN)70, 71, 75
C     NEGATIVE SLOPE OF DIP
70    SHAP(I) = ((X-VXN)*(X-VXN))/(4.*P1) + VYN
      GO TO 40
C     MINIMUM VALUE OF DIP
71    SHAP(I) = VYN
      GO TO 40
C     VERTEX OF DIP TO PHOTO-PEAK
75    IF(I-IXX) 72, 72, 74
72    SHAP(I) = ((X-VXN)*(X-VXN))/(4.*P2) + VYN
      GO TO 40
C     PHOTO-PEAK
74    ARG = ((X-XP)*(X-XP))/(.361*WID*WID)
      IF(ARG-20.) 76, 77, 77
76    SHAP(I) = HIT*EXPF(-ARG)
      GO TO 40
C     SETS SHAP (I) = 0.0 AS THE CALCULATED VALUE WOULD NOT BE SIGNIFICANTLY
C     GREATER THAN 0.0
77    SHAP(I) = 0.0
40    SUM = SUM + SHAP(I)
50    CONTINUE
      IF (sense switch 1) 80, 81
80    CONTINUE
      Do 56 I = I, 166, 5
56    PUNCH 5, SHAP(I), SHAP(I + 1), SHAP(I + 2), SHAP(I + 3), SHAP(I + 4)
      GO TO 45
81    CONTINUE
C     SUMS AND NORMALIZES EACH COLUMN
      Do 41 I = 1, 168
41    SHAP(I) = SHAP(I)/SUM
C     SUMS CHANNELS IN GROUPS OF FOUR
      I = 1
```

TABLE B.1 – (Continued
RESPONSE MATRIX GENERATION

```
      Do 42K = 1, 42
      ASHAP(K) = SHAP(I) + SHAP(I + 1) + SHAP(I + 2) + SHAP(I + 3)
42    I = I + 4
      Do 43 I = 1, 40, 5
43    PUNCH 5, ASHAP(I), ASHAP(I + 1), ASHAP(I + 2), ASHAP(I + 3), ASHAP(I + 4)
      PUNCH 5, ASHAP(41), ASHAP(42)
45    IF (sense switch 2) 44, 60
44    GO TO 6
60    CONTINUE
      END

      SUBROUTINE MARS (VYN, VXN, PECN)
      DIMENSION VX(9),VY(9), PEC(9), GNC(10)
4     FORMAT (F10.5)
      COMMON GNC
      IF (GNC)2)) 14, 14, 17
17    GNC(2) = 0.0
      TYPE 10
10    FORMAT (43H ENTER DATA FOR MARS SUBROUTINE PRESS START)
      PAUSE
      READ 4, (PEC(I), I = 1, 9)
      READ 4, (VX(1), I = 1,9)
      READ 4, (VY(I), I = 1, 9)
14    CONTINUE
      IF (sense switch 1) 96, 97
96    PAUSE
97    CONTINUE
      PE = PECN
      IF(PE- PEC(1)) 2, 3, 3
2     VXN = (PE/PEC(1))*VX(1)
      VYN = (PE/PEC(1))* VY(1)
      GO TO 20
3     DO 6 I = 1,9
      IF (PE-PEC(I))5, 11, 6
6     CONTINUE
11    VXN = VX(I)
      VYN = VY(I)
      GO TO 20
5     PEN = (PE-PEC(I-1))/(PEC(I)-PEC(I-1))
```

TABLE B.1 – (Continued)
RESPONSE MATRIX GENERATION

```
      VXN = PEN*(VX(I)-VX(I-1)) + VX(I-1)
      IF(VY(I)-VY(I-1))8, 9, 9
8     VYN = -(PEN*(VY(I-1)-VY(I))) + VY(I-1)
      GO TO 20
9     VYN = (PEN*(VY(I)-VY(I-1))) + VY(I-1)
20    RETURN
      END
```

TABLE B.2
SPECTRUM UNFOLDING AND ENERGY FLUX CALCULATION

```
      DIMENSION C(42), R(42, 42), D(42), XN(42), XK(42)
3     FORMAT (5F10.0)
5     FORMAT (5E15.7)
13    FORMAT (13, 3X, E14.8)
41    FORMAT (40H)
71    FORMAT (3F15.7)
73    FORMAT (12H EFLUX EQUALS, E14.7)
91    FORMAT (23H SERIES DIVERGENT AT M = 13)
96    FORMAT (F10.8)
      N = 42
      MN = N-2
      L = 50
      DO 6 J = 1, N
      DO 4 I = 1, NN, 5
C     READ RESPONSE MATRIX
4     READ 5, R(I, J), R(I+1, J), R(I+2, J), R(I+3, J), R(I+4, J)
6     READ 5, R(N-1, J), R(N, J)
      DO 95 I = 5, N, 5
95    PRINT 96, R(I, I)
33    READ 41
      WRITE OUTPUT TAPE 4, 41
C     READ INPUT SPECTRUM
1     DO 2 I = 1, NN, 5
2     READ 3, C(I), C(I+1), C(I+2), C(I+3), C(I+4)
C     READ 3, C(N-1), C(N)
      K = N-1
C     INPUT SMOOTHING, IF DESIRED TURN SENSE SWITCH 1 ON IF (sense switch 1) 53, 54
53    DO 51 I = 2, K
51    D(I) = 0.25*C(I-1) + 0.5*C(I) + 0.25*C(I + 1)
      DO 52 I = 1, N
52    C(I) = D(I)
54    DO 8 I = 1, N
8     D(I) = 1.0
      DO 25 M = 1, L
      RS = 0.0
      DO 9 I = 1, N
9     XN(I) = D(1)*C(I)
      DO 10 I = 1, N
```

TABLE B.2 – (Continued)
SPECTRUM UNFOLDING AND ENERGY FLUX CALCULATIONS

```
            A = 0.0
            DO 11 J = 1, N
            XK(1) = R(I, J)*XN(J) + A
11          A = XK(I)
10          D(I) = XN(I)/A
            DO 20 I = 1, N
            RESQ = (XK(I)-C(I))**2 + RS
20          RS = RESQ
            PRINT 13, M, RESQ
            IF (sense switch 3) 69, 81
81          IF (M-1) 25, 25, 22
22          IF (RESQ-REST) 25, 90, 90
25          REST = RESQ
C           OUTPUT SMOOTHING, IF DESIRED TURN ON SENSE SWITCH 2
            IF (sense switch 2) 61, 69
61          DO 68 I = 2, K
68          D(I) = 0.25*XN(I-1)+0.5*XN(1)+0.25*XN(I+1)
            DO 32 I = 1, N
32          XN(I) = D(I)
C           PUNCH IDENTIFICATION
69          PRINT 71, (XN(I), C(I), XK(I), I = 1, N)
            WRITE OUTPUT TAPE 4, 71, (XN(1), C(1), XK(I), I = 1, N)
            EFLUX = 0.0
DO 72 I = 1, N
            CHNR = I
            XN2 = XN(I)*CHNR
            EFLUX = EFLUX + XN2
72          CONTINUE
            WRITE OUTPUT TAPE, 4, 73, EFLUX
C           LOAD NEW DATA
            GO TO 33
90          WRITE OUTPUT TAPE 4, 91, M
            GO TO 69
            END
```

REFERENCES

1. N. E. Scofield, USNRDL Report TR-447, *A Technique for Unfolding Gamma-Ray Scintillation Spectrometer Pulse-Height Distribution,* 24 June 1960.
2. James F. Mollenauer, UCRL-9748, T1D.4500, 16th ed., *A Computer Analysis for Complex Sodium Iodide Gamma Spectra, August 1961.*

CIVIL EFFECTS TEST OPERATIONS REPORT SERIES (CEX)

Through its Division of Biology and Medicine and Civil Effects Test Operations Office, the Atomic Energy Commission conducts certain technical tests, exercises, surveys, and research directed primarily toward practical applications of nuclear effects information and toward encouraging better technical, professional, and public understanding and utilization of the vast body of facts useful in the design of countermeasures against weapons effects. The activities carried out in these studies do not require nuclear detonations.

A complete listing of all the studies now underway is impossible in the space available here. However, the following is a list of all reports available from studies that have been completed. All reports listed are available from the Office of Technical Services, Department of Commerce, Washington 25, D. C., at the prices indicated.

CEX-57.1 ($0.75) The Radiological Assessment and Recovery of Contaminated Areas, Carl F. Miller, September 1960.

CEX-58.1 ($2.75) Experimental Evaluation of the Radiation Protection Afforded by Residential Structures Against Distributed Sources, J. A. Auxier, J. O. Buchanan, C. Eisenhauer, and H. E. Menker, January 1959.

CEX-58.2 ($0.75) The Scattering of Thermal Radiation into Open Underground Shelters, T. P. Davis, N. D. Miller, T. S. Ely, J. A. Basso, and H. E. Pearse, October 1959.

CEX-58.7 ($0.50) AEC Group Shelter, AEC Facilities Division, Holmes & Narver, Inc., June 1960.

CEX-58.8 ($1.00) Comparative Nuclear Effects of Biomedical Interest, Clayton S. White, I. Gerald Bowen, Donald R. Richmond, and Robert L. Corsbie, January 1961.

CEX-58.9 ($1.25) A Model Designed to Predict the Motion of Objects Translated by Classical Blast Waves, I. Gerald Bowen, Ray W. Albright, E. Royce Fletcher, and Clayton S. White, June 1961.

CEX-59.1 ($0.60) An Experimental Evaluation of the Radiation Protection Afforded by a Large Modern Concrete Office Building, J. F. Batter, Jr., A. L. Kaplan, and E. T. Clarke, January 1960.

CEX-59.4 ($1.25) Aerial Radiological Monitoring System. I. Theoretical Analysis, Design, and Operation of a Revised System, R. F. Merian, J. G. Lackey, and J. E. Hand, February 1961.

CEX-59.4 (Pt.II) ($1.50) Aerial Radiological Monitoring System. Part II. Performance, Calibration, and Operational Check-out of the EG&G Arms-II Revised System, J. E. Hand, R. B. Guillou, and H. M. Borella, Oct. 1, 1962.

CEX-59.7B ($1.50) Experimental Radiation Measurements in Conventional Structures. Part II Comparison of Measurements in Above-Ground and Below-Ground Structures from Simulated and Actual Fallout Radiation, Z. G. Burson, January 1964"

CEX-59.7C ($0.50) Methods and Techniques of Fallout Studies Using a Particulate Simulant, William Lee and Henry Borella, February 1962.

CEX-59.13 ($0.50) Experimental Evaluation of the Radiation Protection Afforded by Typical Oak Ridge Homes Against Distributed Sources, T. D. Strickler and J. A. Auxier, April 1960.

CEX-59.14 ($1.75) Determinations of Aerodynamic-drag Parameters of Small Irregular Objects by Means of Drop Tests, E. P. Fletcher, R. W. Albright, V. C. Goldizen, and I. G. Bowen, October 1961.

CEX-60.1 ($1.75) Evaluation of the Fallout Protection Afforded by Brookhaven National Laboratory Medical Research Center, H. Borella, Z. Burson, and J. Jacovitch, February 1961.

CEX-60.3 ($1.50) Extended- and Point-source Radiometric Program, F. J. Davis and P. W. Reinhardt, August 1962.

CEX-60.6 ($1.00) Experimental Evaluation of the Radiation Protection Provided by an Earth-covered Shelter, Z. Burson and H. Borella, February 1962.

CEX-61.1 (Prelim.) Gamma Radiation at the Air-Ground Interface, Keran O'Brien and James E. McLaughlin, Jr., May 29, 1963.

CEX-61.4 ($2.25) Experimental Evaluation of the Fallout-radiation Protection Provided by Selected Structures in the Los Angeles Area, Z. G. Burson, Feb. 26, 1963.

CEX-62.01 ($0.50) Technical Concept—Operation Bren, J. A. Auxier, F. W. Sanders, F. F. Haywood, J. H. Thorngate, and J. S. Cheka, January 1962.

CEX-62.02 ($2.25) Operation Plan and Hazards Report—Operation Bren, F. W. Sanders, F. F. Haywood, M. I. Lundin, L. W. Gilley, J. S. Cheka, and D. R. Ward, April 1962.

CEX-62.03 ($1.00) General Correlative Studies – Operation Bren, J. A. Auxier, F. F. Haywood, L. W. Gilley, September 1963."

CEX-62.2 ($1.00) Nuclear Bomb Effects Computer (Including Slide-rule Design and Curve Fits for Weapons Effects), E. Royce Fletcher, Ray W. Albright, Robert F. D. Perret, Mary E. Franklin, I. Gerald Bowen, and Clayton S. White, Feb. 15, 1963.

CEX-62.81 (Prelim.) ($ 1.25) Ground Roughness Effects on the Energy and Angular Distribution of Gamma Radiation from Fallout, C. M. Huddleston, Z. G. Burson, R. M. Kinkaid, and Q. G. Klinger, May 22, 1963.